NASA TECHNICAL NOTE

NASA TN D-5937

NASA TN D-5937

EFFECTS OF TWO-DIMENSIONAL SINUSOIDAL WAVES ON HEAT TRANSFER AND PRESSURE OVER A PLATE AT MACH 8.0

by Leonard M. Weinstein

Langley Research Center
Hampton, Va. 23365

NATIONAL AERONAUTICS AND SPACE ADMINISTRATION • WASHINGTON, D. C. • AUGUST 1970

1. Report No.	2. Government Accession No.	3. Recipient's Catalog No.
NASA TN D-5937		

4. Title and Subtitle
EFFECTS OF TWO-DIMENSIONAL SINUSOIDAL WAVES ON HEAT TRANSFER AND PRESSURE OVER A PLATE AT MACH 8.0

5. Report Date
August 1970

6. Performing Organization Code

7. Author(s)
Leonard M. Weinstein

8. Performing Organization Report No.
L-5427

10. Work Unit No.
126-13-10-18

9. Performing Organization Name and Address
NASA Langley Research Center
Hampton, Va. 23365

11. Contract or Grant No.

13. Type of Report and Period Covered
Technical Note

12. Sponsoring Agency Name and Address
National Aeronautics and Space Administration
Washington, D.C. 20546

14. Sponsoring Agency Code

15. Supplementary Notes

16. Abstract

An investigation has been conducted to study the effects of multiple two-dimensional sinusoidal waves, arranged normal to flow, on surface heat transfer and pressure distribution over a sharp- or a blunt-leading-edge plate. Surface oil-flow and schlieren photographs were used to define the surface flow and shock structure over the model. The laminar separation lengths in front of the first wave could be correlated by using simple separation concepts. The pressure distributions indicated that the pressure drag would be greater for flow over a distorted surface than over a flat surface at the same flow conditions. For blunt-leading-edge models, the waves tended to trip the flow to early transition. The maximum laminar heating values for laminar flow over multiple waves were found to correlate with empirical parameters obtained from previous investigations. Minimum laminar heating between wave peaks also correlated.

17. Key Words (Suggested by Author(s))
Surface distortions
Laminar separation
Maximum heating
Hypersonic flow

18. Distribution Statement
Unclassified – Unlimited

19. Security Classif. (of this report)	20. Security Classif. (of this page)	21. No. of Pages	22. Price*
Unclassified	Unclassified	42	$3.00

*For sale by the Clearinghouse for Federal Scientific and Technical Information
Springfield, Virginia 22151

EFFECTS OF TWO-DIMENSIONAL SINUSOIDAL WAVES ON HEAT TRANSFER AND PRESSURE OVER A PLATE AT MACH 8.0

By Leonard M. Weinstein
Langley Research Center

SUMMARY

An investigation has been conducted to study the effects of multiple two-dimensional sinusoidal waves, arranged normal to flow, on surface heat transfer and pressure distribution over a sharp- or a blunt-leading-edge plate. Surface oil-flow and schlieren photographs were used to define the surface flow and shock structure over the model. The laminar separation lengths in front of the first wave could be correlated by using simple separation concepts. The pressure distributions indicated that the pressure drag would be greater for flow over a distorted surface than over a flat surface at the same flow conditions. For blunt-leading-edge models, the waves tended to trip the flow to early transition. The maximum laminar heating values for laminar flow over multiple waves were found to correlate with empirical parameters obtained from previous investigations. Minimum laminar heating between wave peaks also correlated.

INTRODUCTION

Surface distortions which occur on hypersonic vehicles may be caused by warping, surface ablation, or structural requirements. For example, some recently proposed thermal-protection systems incorporate uniformly spaced surface protuberances in vehicle design (ref. 1). The surface distortions can greatly affect the local flow and the vehicle surface heating and pressure distributions. The existence of multiple attached and separated viscous layers which interact with the external inviscid flow makes any theoretical analysis of the flow over the distortions a formidable task; thus, a semiempirical prediction approach, whereby experimental results over a wide range of test conditions are correlated, appears attractive.

Several investigations of single surface distortions (for example, refs. 2 to 8) have been made to determine the effect of particular types of protuberances on local surface heating and pressures at supersonic and hypersonic speeds. The effect of one protuberance in the wake of another was examined in reference 3. Multiple two-dimensional distortions were examined in references 9 to 13. The flow was laminar for reference 7,

turbulent for references 3 and 5, and laminar and turbulent for references 2, 4, 6, 8, 9, 10, 11, 12, and 13. Holden (ref. 7) has developed an analytical solution for flow over a wedge and Jaeck (ref. 10) has developed a shallow-wave theory for flow over multiple waves, but the assumptions of these two theories restrict their general usage. Bertram and Wiggs (ref. 2) empirically correlated the maximum laminar heating for single surface distortions; and Bertram, Weinstein, Cary, and Arrington (ref. 9) have extended the correlation to multiple distortions.

The purpose of the present investigation was to study the effects of multiple two-dimensional sinusoidal waves, arranged normal to the flow, on the surface heat transfer and pressure distribution over a sharp- and a blunt-leading-edge plate at a free-stream Mach number of 8.0. By varying stagnation pressure, angle of attack, and nose bluntness, the local Reynolds number per centimeter was varied from 8.3×10^2 to 4.9×10^5 and the local Mach number was varied from 1.8 to 9.2. Flow visualization techniques, consisting of surface oil-flow and schlieren photographs, were utilized at a free-stream Mach number of 6.86 to define the surface flow and shock structure over the model.

SYMBOLS

C_f local skin-friction coefficient

c_p specific heat of air at constant pressure

c_w specific heat of wall material

h heat-transfer coefficient, $\frac{\dot{q}}{T_{aw} - T_w}$

H wave height above flat plate

$\overline{H}$ height above flat plate of reattachment of boundary layer

$\frac{\Delta h}{h_{fp}} = \frac{h_{max} - h_{fp}}{h_{fp}}$

$K_\alpha = M\alpha$

$K_\delta = M\delta$

$K_\theta = M\theta$

$K = K_\alpha + K_\theta$

l_i length of separated region (from separation to reattachment)

L model length

M Mach number

N_{Pr} Prandtl number

N_{St} Stanton number, $\dfrac{\dot{q}}{\rho u c_p (T_{aw} - T_w)}$

p pressure

$\dot{q}$ surface heat-transfer rate

$R_{l,x} = \dfrac{\rho_l u_l x}{\mu_l}$

R_∞ free-stream Reynolds number per centimeter, $\dfrac{\rho_\infty u_\infty}{\mu_\infty}$

$R_{\infty,L} = \dfrac{\rho_\infty u_\infty L}{\mu_\infty}$

t leading-edge thickness

T temperature

u gas velocity

v virtual origin

x surface distance from leading edge or stagnation line

x_v distance to virtual origin of turbulent boundary layer

x' distance along surface of model from beginning of waves

y' perpendicular distance from wall

α plate surface inclination to free-stream flow

$\beta = (M^2 - 1)^{1/2}$

γ ratio of specific heats (1.4 for air)

δ average angle of separated region with respect to flat plate, $\frac{\overline{H}}{l_i}$

δ_l^* local displacement thickness of boundary layer on flat plate

η recovery factor

$\theta = \frac{d\delta_l^*}{dx}$

λ local wall thickness

μ dynamic viscosity

ρ density

τ time

Subscripts:

aw adiabatic wall

fp flat plate

l local conditions at outer edge of boundary layer of smooth plate

max maximum

min minimum

p plateau value in separated region

∞ undisturbed free stream

t stagnation conditions

w wall

APPARATUS AND TEST CONDITIONS

Wind Tunnels

Flow-visualization studies were conducted in the Langley 11-inch hypersonic tunnel at a nominal Mach number of 6.86. This tunnel has a two-dimensional contoured nozzle and an adjustable second minimum with a blowdown operation exhausting to a vacuum sphere. Run time is about 1 minute. The air is preheated to about 620° K to avoid liquefaction. For these studies stagnation pressures of 5, 10, 20, and 40 atmospheres (1 atm = 101.325 kN/m^2) were used; therefore, the free-stream Reynolds number per centimeter varied from 2.4×10^4 to 1.6×10^5 with a corresponding variation of test-section Mach number from 6.7 to 6.9. A more detailed description of this tunnel along with a calibration can be found in reference 14.

Heat-transfer and pressure studies were conducted in the Langley Mach 8 variable-density tunnel. This is also a blowdown tunnel with an axisymmetric contoured nozzle. Stagnation pressures were 4, 15, 55, 70, and 180 atmospheres, and the stagnation temperature was held at about 760° K so that the free-stream Reynolds number per centimeter varied from 10^4 to 3×10^5. The free-stream Mach number in the test section varied from 7.6 to 8.0. This facility is further described in reference 15.

Models

Models used for the oil-flow and schlieren studies at $M_\infty = 6.86$ were constructed of solid metal covered with a layer of epoxy-impregnated fiber glass (the leading edge of the sharp plate was not covered). The models were 10° total-angle wedges with a flat surface on one side and three two-dimensional sinusoidal waves on the other as shown in figure 1. Each wave protruded a maximum of 0.17 cm above and below a section of flat plate preceding and following the waves. The wavelength was 2.54 cm. Sharp ($t \approx 0.005$ cm) and blunt ($t = 1.9$ cm) leading edges were used. End plates shaped to enclose the bow shock were used to reduce cross-flow effects.

Models used for heat-transfer and pressure tests at $M_\infty = 8.0$ were 10° total-angle wedges, 27.94 cm wide and 40.64 cm long, as shown in figure 2. One side of the wedge had five two-dimensional sinusoidal waves preceded and followed by a flat-plate section; the other side of the wedge was completely flat. The waves protruded a maximum of 0.25 cm above and below the flat surface, and the wavelength was 3.8 cm; thus, the ratio

of wave height to wave length was the same as that for the smaller models. Leading-edge thicknesses were the same as those for the oil-flow and schlieren studies. A separate complete model was tested for each leading edge and each type of instrumentation. Chordwise and spanwise locations of instrumentation are listed in table I. End plates shaped to enclose the bow shock were used and are sketched in figure 2.

The heat-transfer models had an inconel wall nominally 0.08 cm thick, insulated from the steel frame by fiber glass. Chromel-alumel thermocouples (diam = 0.025 cm) were spotwelded to the underside of the skin on both sides of the wedge. The wall thickness was accurately measured at each thermocouple location for data-reduction purposes. The pressure models had a stainless-steel wall nominally 0.15 cm thick. Pressure tubes were soldered flush with the wall and had an orifice nominally 0.25 cm in diameter.

EXPERIMENTAL PROCEDURES

Flow Visualization

For the oil-flow tests a mixture of oil and lampblack was dotted on the model surface. The tunnel flow was started with a quick-opening valve, the model was exposed to the flow at $M_\infty = 6.86$ for about 5 seconds, and the valve was then closed. The model was subsequently photographed to record the surface oil-flow pattern. Separation and reattachment locations were indicated by oil accumulation lines and scoured regions, respectively.

The same models used in the oil-flow tests were used without end plates to make schlieren photographs of the flow field. A single-pass schlieren system was used with a mercury arc lamp source.

Heat-Transfer Measurements

The conventional thin-skin transient-heating technique was used to obtain heat-transfer distributions at $M_\infty = 8.0$. The models, which were initially at room temperature, were injected into a fully established airflow in about 0.25 second with less than 0.10 second to traverse the tunnel boundary layer.

Pressure Measurements

Two types of pressure transducers were used for the pressure-distribution study. One was a vacuum thermocouple gage with a range from 0.05 to 1.4 kN/m^2 and was used for the lower pressures. The other transducers were metal diaphragm gages with full-scale ranges of 7 kN/m^2, 14 kN/m^2, and 35 kN/m^2.

Tests

The conditions for the tests of this investigation are given in table II. The local Mach number for these tests was varied by changing the angle of attack and the leading-edge diameter. The local Mach number, which varied slightly with Reynolds number, was calculated by using the oblique-shock relations (including model surface angle plus the boundary-layer displacement effects) for the sharp leading edge and by assuming that the boundary layer for the blunt-leading-edge plate is immersed in the high-entropy layer due to the normal part of the detached leading-edge shock. For the blunt-leading-edge pressure distribution, the blast-wave correlation of reference 16 was used. The calculated values of local Mach number are given in table III.

DATA REDUCTION

Heat Transfer

The voltage produced by the thermocouples was sampled 20 times a second, converted to a binary digital system, and recorded on magnetic tape. The temperature at the reference junction of the thermocouple was measured by a thermometer and did not vary noticeably during a run. The reference temperature and calibration for the thermocouple wire were used to reduce the electrical outputs of the thermocouples to temperatures. After the model was positioned in the flow, 0.5 second of the temperature-time data (10 data points) was recorded. The data were fitted to a second-degree polynomial curve by the least-squares method. In the absence of conduction and radiation errors, heat transfer was calculated by using the initial slope $\frac{dT_w}{d\tau}$ of the temperature-time curve in the thin-wall equation

$$\dot{q} = c_w \rho_w \lambda \frac{dT_w}{d\tau}$$

where

$$c_w = 372 + 0.252T_w \qquad (J/kg\text{-}^oK)$$

and model wall density ρ_w is 8540 kg/m^3. Radiation and conduction heat losses were calculated and found to be negligible when compared with convective heating. The Stanton number was computed by using the equation

$$N_{St,\infty} = \frac{\dot{q}}{\rho_\infty u_\infty c_p (T_{aw} - T_w)}$$

where the adiabatic-wall temperature was found from the relation

$$T_{aw} = T_t \frac{1 + \eta \frac{\gamma - 1}{2} M_l^2}{1 + \frac{\gamma - 1}{2} M_l^2}$$

The recovery factor η was taken as 0.845 for laminar flow and 0.89 for turbulent flow.

Pressure

The voltage produced by the pressure transducers was converted to a binary digital system and recorded on magnetic tape. A calibration curve was supplied for each transducer, and the data were converted to pressures. Outputs from the vacuum thermocouple transducer are highly nonlinear, and pressure errors may be as great as 5 percent of the full range. The metal diaphragm transducer is accurate within about 0.5 percent of the full range and was used for most of the tests in this investigation.

RESULTS AND DISCUSSION

Flow Visualization

Representative oil-flow and schlieren photographs are shown in figure 3 for the sharp- and blunt-leading-edge models. An analysis of the photographs indicates that the boundary layer separates in front of the first wave and subsequently reattaches to the face of that wave. The flow remains attached over the top of the wave. As the flow expands over the rear of the first wave, the boundary layer again separates and then reattaches on the face of the second wave. This separation-reattachment process continues over the remaining waves until the boundary layer reattaches to the flat section of the plate behind the last wave.

The effect of end plates on separation length ahead of the first wave was determined from oil-flow studies by using the blunt model at an angle of attack of 15°. As indicated by figure 4, the separation length near the model center line is approximately the same with or without end plates; however, away from the center line there are marked differences. For the model with end plates, edge or corner effects apparently occur only at the edge of the first distortion. In the separated region preceding the third distortion, the oil appears to accumulate in distinct cell-like patterns across the entire model. (This phenomenon is also depicted in ref. 12.) Removal of end plates eliminated these patterns but produced a strong outflow. Heat-transfer data presented later in this report indicate that the flow was transitional at the second wave; therefore, the cell-like patterns may be related to the occurrence of transition and/or to edge or corner effects.

A correlation of the separation length to the first wave determined from oil-flow studies is presented in figure 5 for laminar flow preceding the first wave. The correlation parameters used in figure 5 are derived in the appendix.

All of the terms in the correlation parameter are undisturbed flat-plate values except $\overline{H}$ and l_i. If it is assumed that $\overline{H} \approx H$ (oil-flow and schlieren studies indicate that this assumption is valid for the present investigation), the separation length can be obtained from the correlation.

Values of $\overline{H}$ and of l_i measured in the oil-flow study and theoretical values of M_l and $R_{l,x}$ were used to reduce the separation-length data to the coordinates of figure 5. Equation (A3) predicts the trend of the experimental data well, but the predicted values fall 15 percent below the mean of the experimental data.

Surface Pressures

Ratios of the measured wall pressures to the undisturbed free-stream static pressures are presented as a function of the distance x in figures 6 and 7 for the sharp- and blunt-leading-edge models, respectively. The stagnation-point location for the blunt-leading-edge model varies with angle of attack, and thus the distance x to a given instrument location also varies with angle of attack.

Flat surface.- The theoretical pressures for flat plates with sharp leading edges (fig. 6) were obtained from the hypersonic oblique-shock equation given in reference 17:

$$\frac{\Delta p}{p_\infty} = 2.333\left(0.36K^2 + 0.6K\sqrt{1 + 0.36K^2}\right) \qquad (K \geqq 0) \qquad (1)$$

where $K = K_\alpha + K_\theta$ and includes the total inclination of the flow. The value of K_θ was found by assuming weak interaction and using the boundary-layer formulation in reference 18, where the boundary-layer growth parameter was calculated from $G = 0.344\left(\frac{T_w}{T_{aw}} + 0.352\right)$ for $\gamma = 1.4$ and $N_{Pr} = 0.725$. The theoretical pressures for flat plates with blunt leading edges were predicted by using the blast-wave correlation of reference 16 and are shown in figure 7.

Generally good agreement between flat-plate theory and data can be seen in both figures 6 and 7. The pressures on the flat surfaces ahead of the first separation and behind the final reattachment on the distortion side also generally agree with flat-plate theory and data.

Multiple-wave surface.- The pressure distributions over the multiple-wave surfaces shown in figures 6 and 7 are characterized by a series of maximum and minimum

pressure peaks as the flow traverses the five waves. A pressure peak occurs a small distance after the reattachment point indicated by the oil-flow studies (also in agreement with refs. 12 and 13). The onset of transitional and turbulent flow evidently causes the pressure variation to become greater. The peak pressures generally decrease from wave peak to wave peak for laminar flow (fig. 6(a), $\alpha = 10^{\circ}$) or turbulent flow (fig. 6(b), $\alpha = 15^{\circ}$, $x > x_v$) but increase for transitional flow (fig. 6(a), $\alpha = 15^{\circ}$, $x < x_v$) over the waves. The magnitude of the pressure peaks is generally larger for transitional and turbulent flow than for laminar flow because the flow turning angle on the face of the wave is greater for turbulent flow.

If the pressure is integrated over the surface and the forces are referenced to the model axis, the pressure drag can be obtained. The pressure drag for laminar flow over the distortions when $\alpha = 10^{\circ}$ (fig. 6(a)) is about 50 percent higher than the flat-plate value. For transitional-turbulent flow when $\alpha = 10^{\circ}$ (fig. 6(b)), the pressure drag is more than double the flat-plate value. The large increase in pressure drag, especially the greater increase in transitional-turbulent pressure drag, may be important.

Surface Heating

Heat-transfer data are shown in figure 8 for the sharp-leading-edge model and in figure 9 for the blunt-leading-edge model. Stanton number based on free-stream conditions is shown as a function of distance from the leading edge or stagnation line. For this investigation, the boundary layer was usually laminar at the first few instrumented locations on all models. On the flat plate the region of transitional heating is characterized by increasing values of $N_{St,\infty}$ with distance x; on the multiple-wave surface, by increasing peak heating values with distance from v (fig. 8(c), $\alpha = 5^{\circ}$). For both laminar and turbulent flow, the maximum heating over successive waves decreases. (See fig. 8(a), $\alpha = 5^{\circ}$, for laminar flow and fig. 8(e), $\alpha = 5^{\circ}$, $x > x_v$, for turbulent flow.)

There was some spanwise variation in the location of transition. (See fig. 8(c), $\alpha = 10^{\circ}$, for example.) The data at the different spanwise locations were faired separately and two smooth curves were obtained. This variation may be due to nonuniformity in the model leading-edge thickness (or leading-edge roughness) for the sharp-leading-edge model and/or irregularities in the model surface due to thermal warping during a run for either the sharp- or the blunt-leading-edge model.

Flat surface.- Laminar flat-plate skin friction for the sharp-leading-edge model was calculated by using the T-prime method of Monaghan (ref. 19) along with the Blasius equation for laminar skin friction. Skin friction was converted to heat transfer by using Colburn's form of Reynolds analogy $\frac{2N_{St}}{C_f} = N_{Pr}^{-2/3}$ where the Prandtl number (ref. 20)

was based on the laminar T-prime temperature. Surface heating for the blunt-leading-edge model was calculated by using the same equations with the local-flow conditions. The predicted laminar values of Stanton number shown in figures 8 and 9 generally agree well with the laminar flat-plate data.

Computation of turbulent Stanton numbers requires that the location of a "virtual origin" of the turbulent boundary layer be known. This virtual origin v was assumed to be the location of peak heating near the end of transition for the flat plate or the maximum of a fairing through the heating peaks over successive waves for the distorted side. (See ref. 12 for details.) Monaghan's T-prime method for turbulent flow (ref. 18) was used with the Kármán-Schoenherr equations as given in reference 21 to calculate the local skin-friction coefficient. Colburn's form of Reynolds analogy, for which the Prandtl number was based on the turbulent T-prime temperature, was used to convert skin-friction coefficients to heat-transfer coefficients. Turbulent-heating predictions using the T-prime method are included where applicable in figures 8 and 9. These turbulent predictions generally agree in level with the experimental turbulent-heating data, the best agreement being obtained for the lower local Mach numbers which correspond to $\alpha = 5^{\circ}$, 10°, and 15°.

Multiple-wave surface.- There is reasonably good agreement between flat-plate heating data and the data for the flat portions of the distorted side ahead of separation at the first wave and after reattachment behind the last wave except when the distortion tripped the flow to early transition. Although the sinusoidal waves did not generally promote early transition on the sharp-leading-edge model (fig. 8), they frequently tripped the boundary layer of the blunt-leading-edge model (fig. 9), probably because the local Mach number was substantially lower (M_l = 1.8 to 3.2) than for the sharp-leading-edge model (M_l = 4.4 to 9.2). Flow at the lower Mach numbers has been observed to be far easier to trip. (For example, see ref. 22.)

For laminar flow at the first wave (a majority of cases for this study) the maximum heating on the wave is shown in figure 10 correlated with the parameter $\frac{M_l}{\delta_l^*/H}$, which was suggested in reference 2 though the constants were subsequently modified in reference 9. It should be pointed out that these data were used in reference 9 to aid in evaluating the constants, and other comparisons are contained in references 12 and 13. The correlation curve recommended in reference 9 is shown in figure 10 and agrees fairly well with the data of the present study. A possible fairing of the present data is represented by the solid line for $\frac{\Delta h}{h_{fp}} = 0.032\left(\frac{M_l}{\delta_l^*/H}\right)^{1.7}$. Appendix A of reference 10 presents the shallow-wave theory which predicts peak heating on two-dimensional waves in attached supersonic

flow. Values of $\frac{\Delta h}{h_{fp}}$ calculated by using this theory for two local Mach numbers are shown in figure 10. Agreement of results from the shallow-wave theory with the present experimental data is generally poor. Since the development of shallow-wave theory required that there be no separation prior to the wave, it is not surprising that this theory does not agree with the data.

Maximum heating data for the first wave and for subsequent waves over which the flow appeared to be laminar are presented in figure 11. The values of M_l and δ_l^* were calculated at the x location of each peak by assuming the wavy surface was flat. The maximum laminar heating values for the waves downstream of the first wave are generally above the correlation curve for the first-peak data, and the disagreement with the first-wave correlation appears to increase from the second to the fifth wave. This behavior might be expected since disturbances from the waves tend to alter the local flow conditions. However, the difference between the first-wave value and the value for subsequent waves is not great, and the correlation for the first-wave maximum heating can be used as a first approximation for maximum heating on multiple waves.

Minimum laminar heating between the wave peaks has also been correlated by using parameters suggested by the maximum heating correlation and is shown in figure 12 as the plot of $\frac{h_{min}}{h_{fp}}$ against $\frac{M_l}{\delta_l^*/H}$. In this figure, the minimum heating is considered only for laminar flow and only behind the first four peaks since the flat plate behind the last peak corresponds to a different geometry. The curve which provides the best overall fit to the data is $\frac{h_{min}}{h_{fp}} = 0.94\left(\frac{M_l}{\delta_l^*/H}\right)^{-1}$. The large data scatter in figure 12 is partly due to lower accuracy of the heat transfer for these very low heating rates.

CONCLUSIONS

An investigation has been conducted to study the effects of multiple two-dimensional sinusoidal waves embedded in a flat surface on the surface flow at a Mach number of 6.86 and the heat transfer and pressure distribution at a Mach number of 8.0. Sharp- and blunt-leading-edge models were inclined at surface angles of attack of -5°, 0°, 5°, 10°, and 15°, resulting in a local Mach number range from 1.8 to 9.2. Variation of the stagnation pressure provided a local Reynolds number per centimeter which varied from 8.3×10^2 to 4.9×10^5. The model wall temperature for the heat-transfer study was approximately 0.4 of the free-stream total temperature. Results of the investigation indicate the following conclusions:

1. Laminar flow over the first wave peak results in separation lengths that can be correlated by using simple separation concepts.

2. The pressure distribution over the multiple-wave surface indicates that the distortions increase pressure drag. In a typical case the pressure drag for laminar flow over the distorted surface was 50 percent greater than the flat-plate value; for transitional-turbulent flow, pressure drag was more than double the flat-plate value.

3. For blunt-leading-edge models, the waves tended to trip the flow to early transition. This tripping is caused by the low local Mach number.

4. Maximum heating values for laminar flow over multiple waves were found to correlate with empirical parameters obtained from other investigations. The correlation for multiple waves indicated that, at least as a first approximation, each wave can be examined as if it stood alone.

5. Minimum heating between wave peaks in laminar flow has also been correlated by using parameters suggested by the maximum heating correlation.

Langley Research Center,
National Aeronautics and Space Administration,
Hampton, Va., May 26, 1970.

APPENDIX

PREDICTION OF LAMINAR SEPARATION LENGTH

Idealized laminar flow separation over a small two-dimensional wave is shown schematically below:

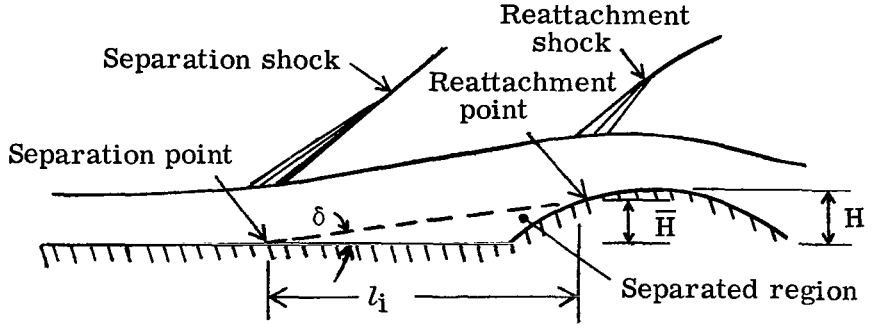

Several studies have shown that the pressure in the separated region can be calculated by assuming that the separated region is a small solid wedge (for example, refs. 4 and 7). In other studies (for example, ref. 23), it is shown that the plateau pressure coefficient in the separated region in front of a wave can be empirically related to M_l and $R_{l,x}$. The correlation equation given as equation (7) of reference 23 is used herein. This relation can be written as

$$\frac{p_p}{p_l} = 1 + 1.27 \frac{M_l^2}{\beta_l^{1/2} R_{l,x}^{1/4}} \qquad (\gamma = 1.4) \qquad \text{(A1)}$$

The small-wedge approximation of reference 17 gives these pressures in terms of the flow turning angle:

$$\frac{p_p}{p_l} = 1 + 2.333\left(0.36K_\delta^2 + 0.6K_\delta\sqrt{1 + 0.36K_\delta^2}\right) \qquad \left(\gamma = 1.4; \quad K_\delta \geqq 0\right) \qquad \text{(A2)}$$

where $K_\delta = M_l\delta$. Since $\delta \approx \frac{\bar{H}}{l_i}$, equations (A1) and (A2) may be combined to get:

$$1.27 \frac{M_l^2}{\beta_l^{1/2} R_{l,x}^{1/4}} = 0.84\left(M_l \frac{\bar{H}}{l_i}\right)^2 + 1.40\left(M_l \frac{\bar{H}}{l_i}\right)\sqrt{1 + 0.36\left(M_l \frac{\bar{H}}{l_i}\right)^2} \qquad \text{(A3)}$$

which can be solved for the separated length if the local flow conditions and $\bar{H}$ are known.

REFERENCES

1. Jackson, L. Robert; Davis, John G., Jr.; and Wichorek, Gregory R.: Structural Concepts for Hydrogen-Fueled Hypersonic Airplanes. NASA TN D-3162, 1966.

2. Bertram, Mitchel H.; and Wiggs, M. Margarette: Effect of Surface Distortions on the Heat Transfer to a Wing at Hypersonic Speeds. AIAA J., vol. 1, no. 6, June 1963, pp. 1313-1319.

3. Burbank, Paige B.; Newlander, Robert A.; and Collins, Ida K.: Heat-Transfer and Pressure Measurements on a Flat-Plate Surface and Heat-Transfer Measurements on Attached Protuberances in a Supersonic Turbulent Boundary Layer at Mach Numbers of 2.65, 3.51, and 4.44. NASA TN D-1372, 1962.

4. Chapman, Dean R.; Kuehn, Donald M.; and Larson, Howard K.: Investigation of Separated Flows in Supersonic and Subsonic Streams With Emphasis on the Effect of Transition. NACA Rep. 1356, 1958. (Supersedes NACA TN 3869.)

5. Murphy, Ed: Heat Transfer in the Vicinity of a Two-Dimensional Protuberance. NASA TM X-53257, 1965.

6. Sterrett, J. R.; and Holloway, P. F.: On the Effect of Transition on Parameters Within a Separation Region at Hypersonic Speeds – With Emphasis on Heat Transfer. Symposium on Fully Separated Flows, Arthur G. Hansen, ed., Amer. Soc. Mech. Eng., May 1964, pp. 15-26.

7. Holden, Michael S.: Experimental Studies of Separated Flows at Hypersonic Speeds. Part II: Two-Dimensional Wedge Separated Flow Studies. AIAA J., vol. 4, no. 5, May 1966, pp. 790-799.

8. Holloway, Paul F.; Sterrett, James R.; and Creekmore, Helen S.: An Investigation of Heat Transfer Within Regions of Separated Flow at a Mach Number of 6.0. NASA TN D-3074, 1965.

9. Bertram, M. H.; Weinstein, L. M.; Cary, A. M., Jr.; and Arrington, J. P.: Heat Transfer to Wavy Wall in Hypersonic Flow. AIAA J., vol. 5, no. 10, Oct. 1967, pp. 1760-1767.

10. Jaeck, C. L. (With appendix A by R. T. Savage and A. L. Nagel): Analysis of Pressure and Heat Transfer Tests on Surface Roughness Elements With Laminar and Turbulent Boundary Layers. NASA CR-537, 1966.

11. Shore, Charles P.; Dixon, Sidney C.; and Griffith, George E.: Experimental Pressures and Turbulent Heat-Transfer Coefficients Associated With Sinusoidal Protuberances on a Flat Plate at a Mach Number of 3. NASA TN D-1626, 1963.

12. Cary, Aubrey M., Jr.; and Morrisette, E. Leon: Effect of Two-Dimensional Multiple Sine-Wave Protrusions on the Pressure and Heat-Transfer Distributions for a Flat Plate at Mach 6. NASA TN D-4437, 1968.

13. Arrington, James P.: Heat-Transfer and Pressure Distributions Due to Sinusoidal Distortions on a Flat Plate at Mach 20 in Helium. NASA TN D-4907, 1968.

14. Bertram, Mitchel H.: Exploratory Investigation of Boundary-Layer Transition on a Hollow Cylinder at a Mach Number of 6.9. NACA Rep. 1313, 1957. (Supersedes NACA TN 3546.)

15. Stainback, P. Calvin: Heat-Transfer Measurements at a Mach Number of 8 in the Vicinity of a 90° Interior Corner Alined With the Free-Stream Velocity. NASA TN D-2417, 1964.

16. Baradell, Donald L.; and Bertram, Mitchel H.: The Blunt Plate in Hypersonic Flow. NASA TN D-408, 1960.

17. Bertram, Mitchel H.: Hypersonic Laminar Viscous Interaction Effects on the Aerodynamics of Two-Dimensional Wedge and Triangular Planform Wings. NASA TN D-3523, 1966.

18. Monaghan, R. J.: On the Behaviour of Boundary Layers at Supersonic Speeds. Fifth International Aeronautical Conference, Rita J. Turino and Caroline Taylor, eds., Inst. Aeron. Sci., Inc., June 1955, pp. 277-315.

19. Monaghan, R. J.: An Approximate Solution of the Compressible Laminar Boundary Layer on a Flat Plate. R & M No. 2760, Brit. A.R.C., 1953.

20. Hilsenrath, Joseph: The NBS-NACA Tables of Thermal Properties of Gases. Table 2.44 Dry Air – Prandtl Number. Nat. Bur. Stand., U.S. Dep. Com., July 1950.

21. Peterson, John B., Jr.: A Comparison of Experimental and Theoretical Results for the Compressible Turbulent-Boundary-Layer Skin Friction With Zero Pressure Gradient. NASA TN D-1795, 1963.

22. Holloway, Paul F.; and Sterrett, James R.: Effect of Controlled Surface Roughness on Boundary-Layer Transition and Heat Transfer at Mach Numbers of 4.8 and 6.0. NASA TN D-2054, 1964.

23. Sterrett, James R.; and Emery, James C.: Extension of Boundary-Layer-Separation Criteria to a Mach Number of 6.5 by Utilizing Flat Plates With Forward-Facing Steps. NASA TN D-618, 1960.

TABLE I.- LOCATION OF MODEL INSTRUMENTATION

[L = 40.6 cm[2]]

Thermocouple	x/L (a)	Thermocouple	x/L
T1	0.0748	T47	0.3250
T2	.1050	T48	.3363
T3	.1362	T49	.3438
T4	.1675	T50	.3575
T5	.1988	T51	.3688
T6	.1988	T52	.3825
T7	.1988	T53	.4075
T8	.2300	T54	.4188
T9	.2612	T55	.4300
T10	.2915	T56	.4514
T11	.3238	T57	.4625
T12	.3550	T58	.4764
T13	.3864	T59	.5010
T14	.4175	T60	.5063
T15	.4487	T61	.5125
T16	.4487	T62	.5238
T17	.4487	T63	.5315
T18	.4802	T64	.5450
T19	.5110	T65	.5563
T20	.5425	T66	.5698
T21	.5738	T67	.5698
T22	.6365	T68	.5698
T23	.6985	T69	.5950
T24	.7614	T70	.6063
T25	.8235	T71	.6173
T26	.8860	T72	.6490
T27	.8860	T73	.6500
T28	.8860	T74	.6638
T29	.8860	T75	.6890
T30	.9490	T76	.6940
T31	.0662	T77	.7000
T32	.0975	T78	.7110
T33	.1294	T79	.7190
T34	.1607	T80	.7376
T35	.1767	T81	.7530
T36	.1918	T82	.7690
T37	.2075	T83	.7845
T38	.2075	T84	.8158
T39	.2075	T85	.8470
T40	.2232	T86	.8780
T41	.2388	T87	.9095
T42	.2700	T88	.9410
T43	.2857	T89	.9718
T44	.3013	T90	.9718
T45	.3138	T91	.9718
T46	.3178	T92	.9718

Pressure orifice	x/L (a)	Pressure orifice	x/L (a)
P1	0.0432	P33	0.4300
P2	.0903	P34	.4513
P3	.1368	P35	.4625
P4	.1994	P36	.4762
P5	.2619	P37	.5010
P6	.3245	P38	.5125
P7	.4495	P39	.5238
P8	.4495	P40	.5450
P9	.4495	P41	.5450
P10	.5744	P42	.5450
P11	.6993	P43	.5563
P12	.8240	P44	.5698
P13	.8860	P45	.5950
P14	.8860	P46	.6063
P15	.8860	P47	.6173
P16	.9490	P48	.6490
P17	.1594	P49	.6500
P18	.1751	P50	.6638
P19	.2063	P51	.6890
P20	.2218	P52	.7000
P21	.2375	P53	.7110
P22	.2688	P54	.7260
P23	.2844	P55	.7428
P24	.3000	P56	.7577
P25	.3138	P57	.7890
P26	.3187	P58	.8202
P27	.3363	P59	.8514
P28	.3575	P60	.8830
P29	.3687	P61	.9140
P30	.3824	P62	.9450
P31	.4075	P63	.9450
P32	.4187	P64	.9450
		P65	.9765

[a]Length L based on sharp-leading-edge model.

TABLE II.- TEST CONDITIONS

M_∞	Leading edge	Type of data	α, deg	R_∞, per cm	$\frac{T_w}{T_t}$
6.86	Sharp and blunt	Oil flow and schlieren	-5, 0, 5, 10, 15	0.024×10^6 .042 .084 .16	0.5 to 0.8
8.0	Sharp	Heat transfer	-5, 0, 5, 10, 15	0.010×10^6 .032 .11 .30	0.4
8.0	Blunt	Heat transfer	0, 5, 10	0.032×10^6 .11 .13 .30	0.4
8.0	Sharp	Pressure	5, 10, 15	0.032×10^6 .13	0.84
8.0	Blunt	Pressure	0, 5, 10	0.032×10^6 .13	0.84

TABLE III.- LOCAL MACH NUMBER

M_∞	Leading edge	α, deg	M_l
6.86	Sharp	-5	8.0
		0	6.8
		5	6.0
		10	5.2
		15	4.4
6.86	Blunt	-5	2.4 to 3.0
		0	2.2 to 2.8
		5	2.0 to 2.5
		10	1.9 to 2.3
		15	1.8 to 2.1
8.0	Sharp	-5	9.2
		0	8.0
		5	6.9
		10	5.8
		15	4.7
8.0	Blunt	0	2.5 to 3.2
		5	2.3 to 2.8
		10	2.0 to 2.4

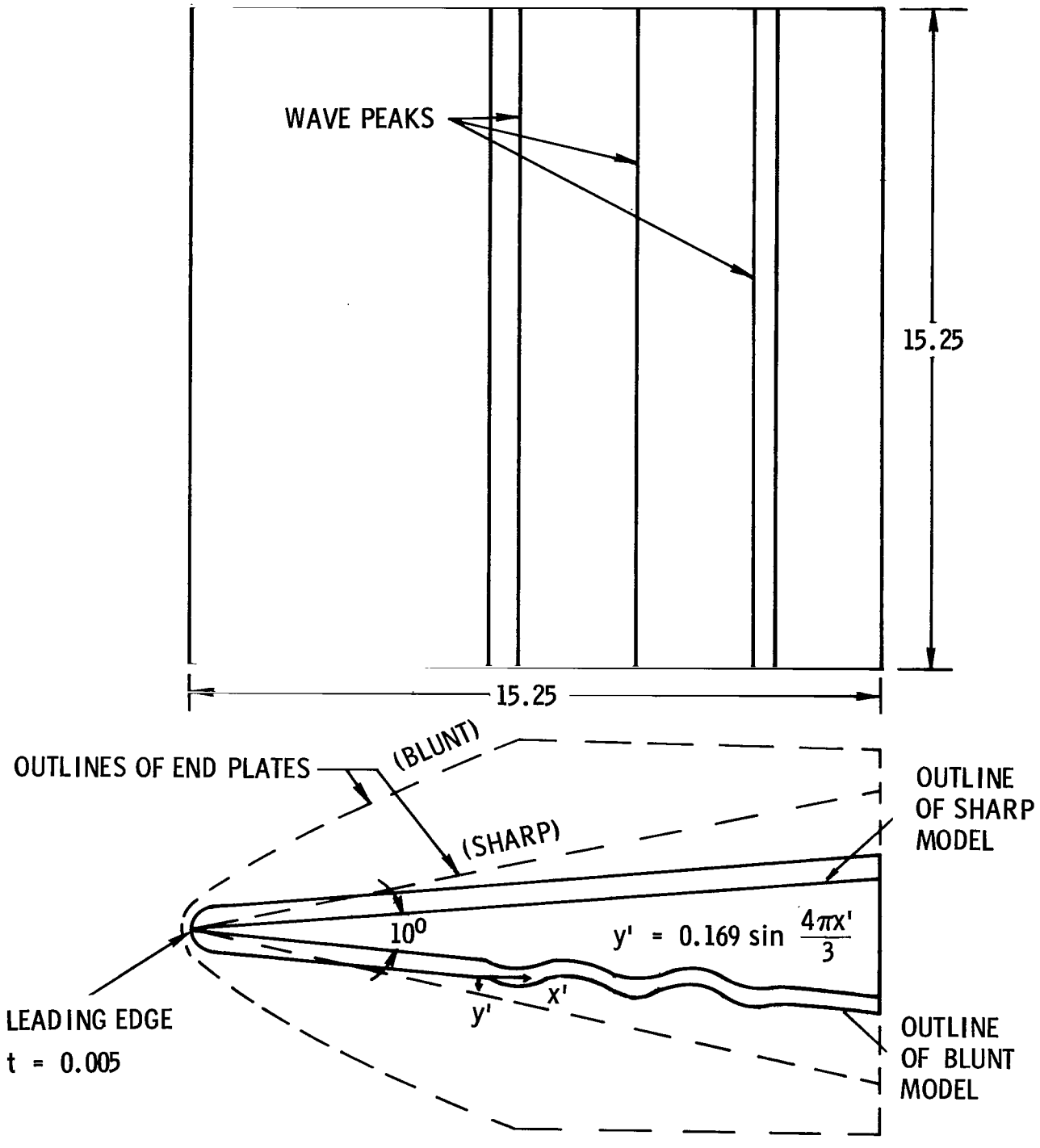

Figure 1.- Models used for oil-flow and schlieren studies at $M_\infty = 6.86$. Dimensions are in centimeters.

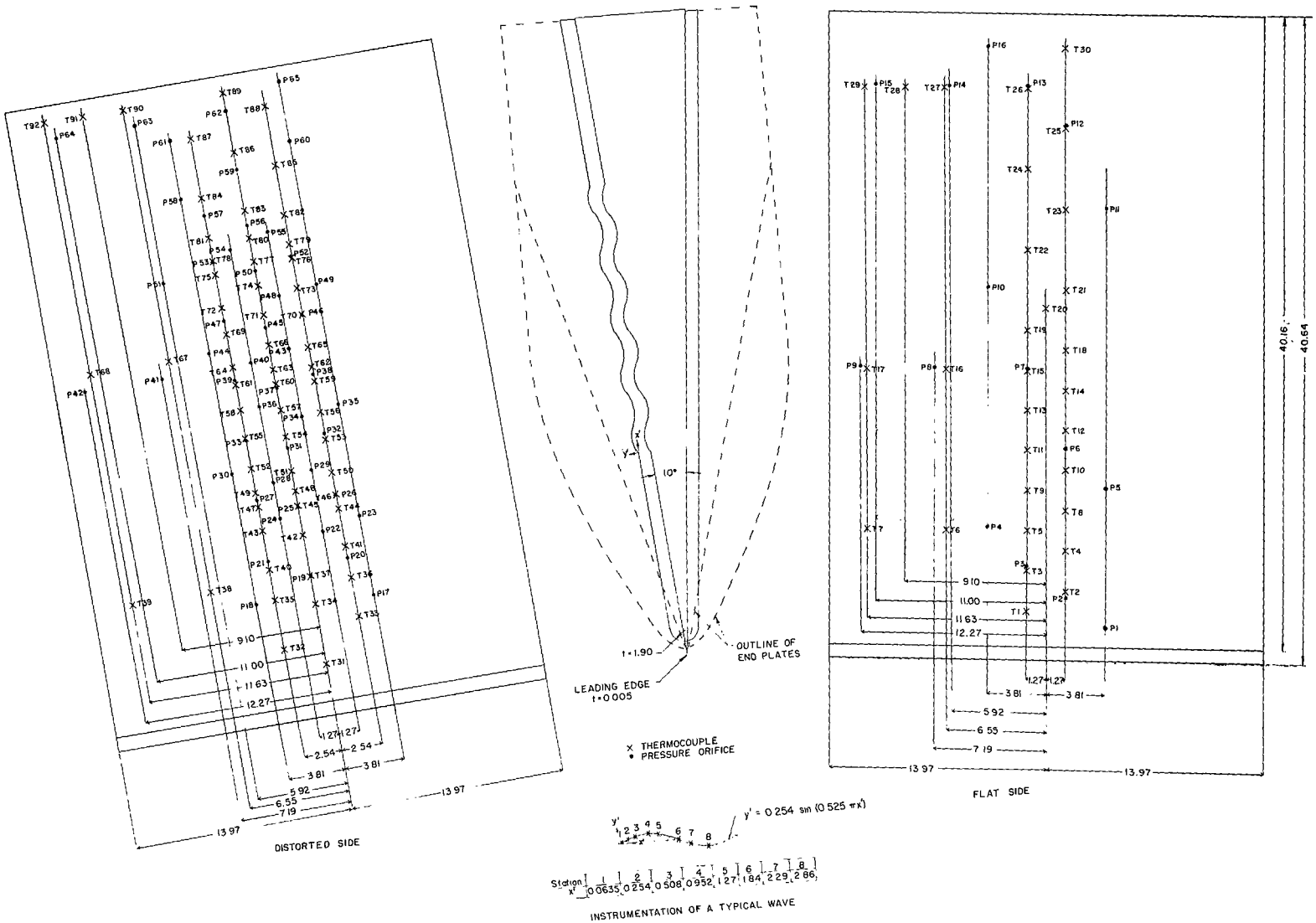

Figure 2.- Model used for heat-transfer and pressure tests at $M_\infty = 8.0$. Dimensions are in centimeters.

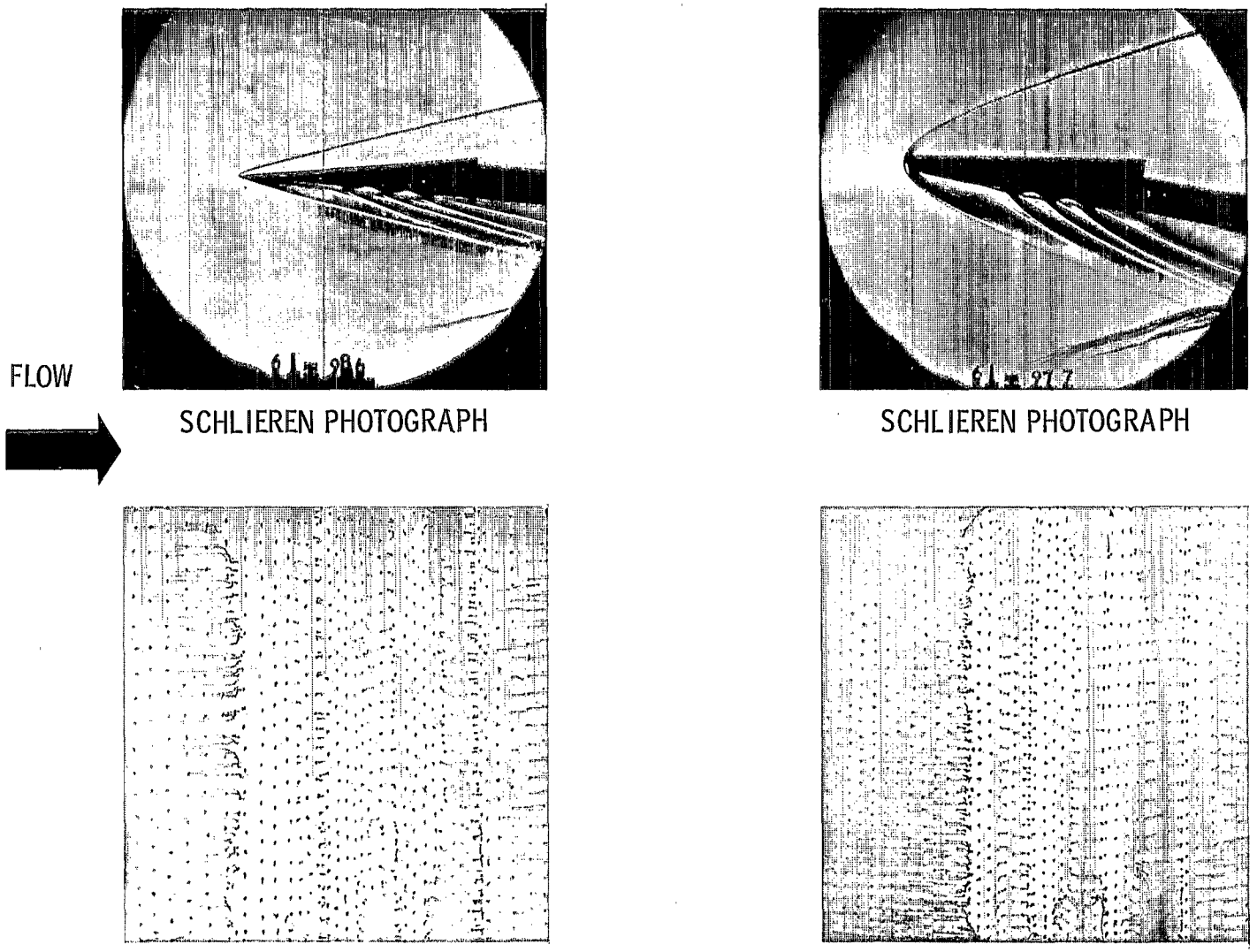

(a) Sharp-leading-edge model. $\alpha = 5^{0}$, distorted side.

(b) Blunt-leading-edge model. $\alpha = 10^{0}$, distorted side.

Figure 3.- Visualization of hypersonic flow over two-dimensional sinusoidal waves. $M_{\infty} = 6.86$; $R_{\infty,L} = 2.1 \times 10^{6}$. L-70-1638

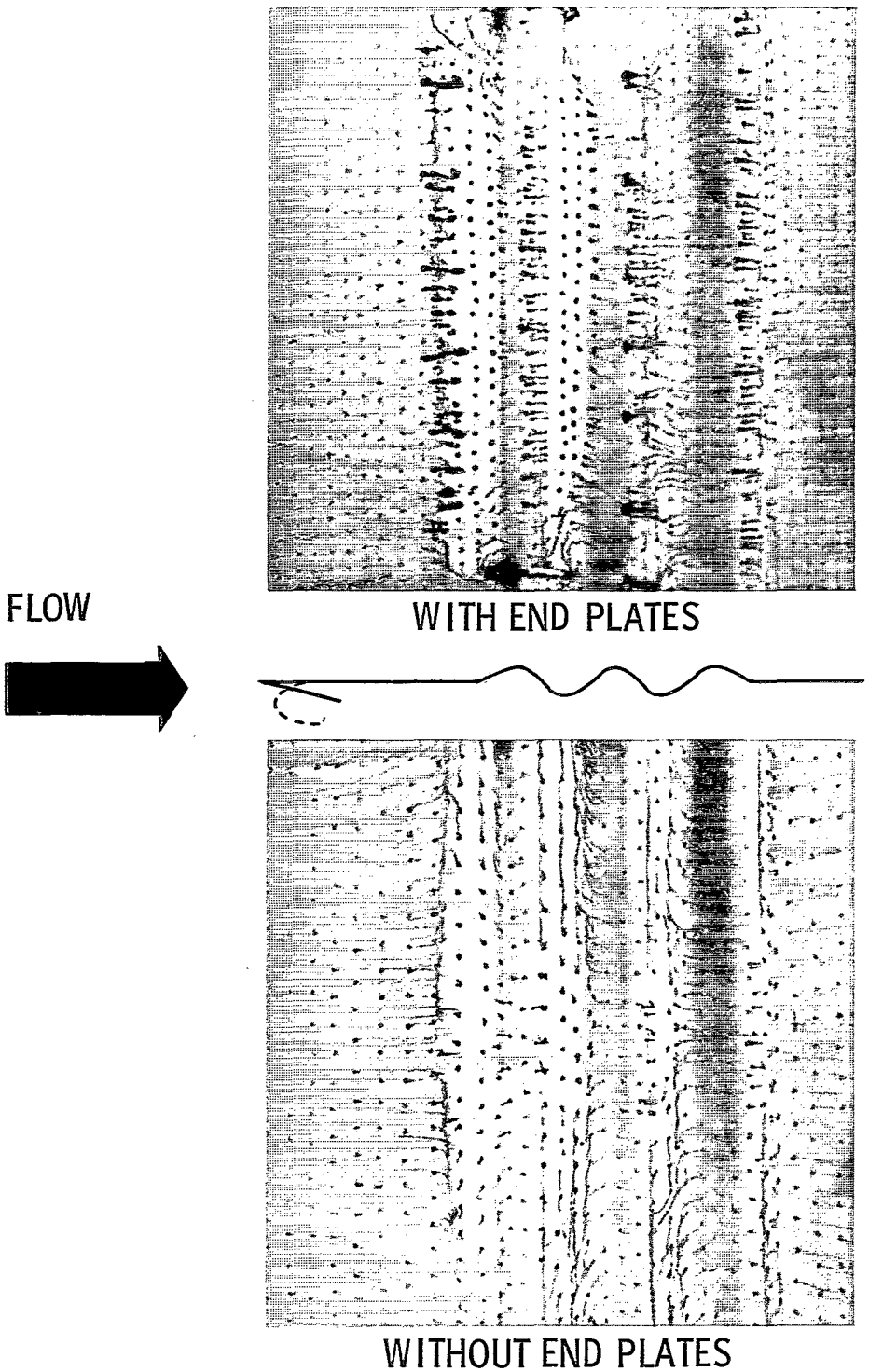

Figure 4.- Oil-flow patterns for multiple-wave surface with blunt leading edge. $M_\infty = 6.86$; $R_{\infty,L} = 1.2 \times 10^6$; $\alpha = 15^0$. L-70-1639

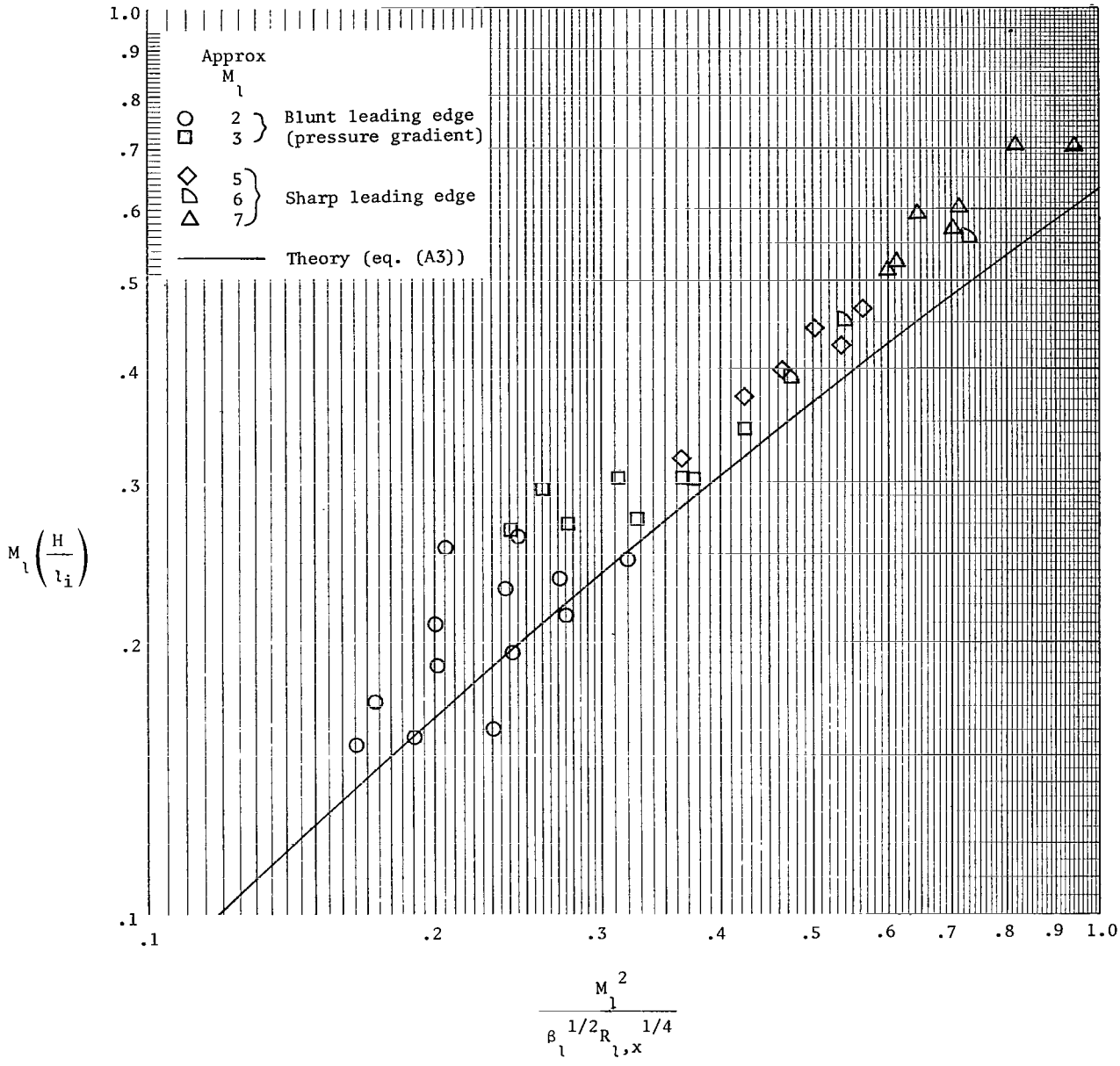

Figure 5.- Correlation of separation length to first wave for laminar flow. $M_\infty = 6.86$.

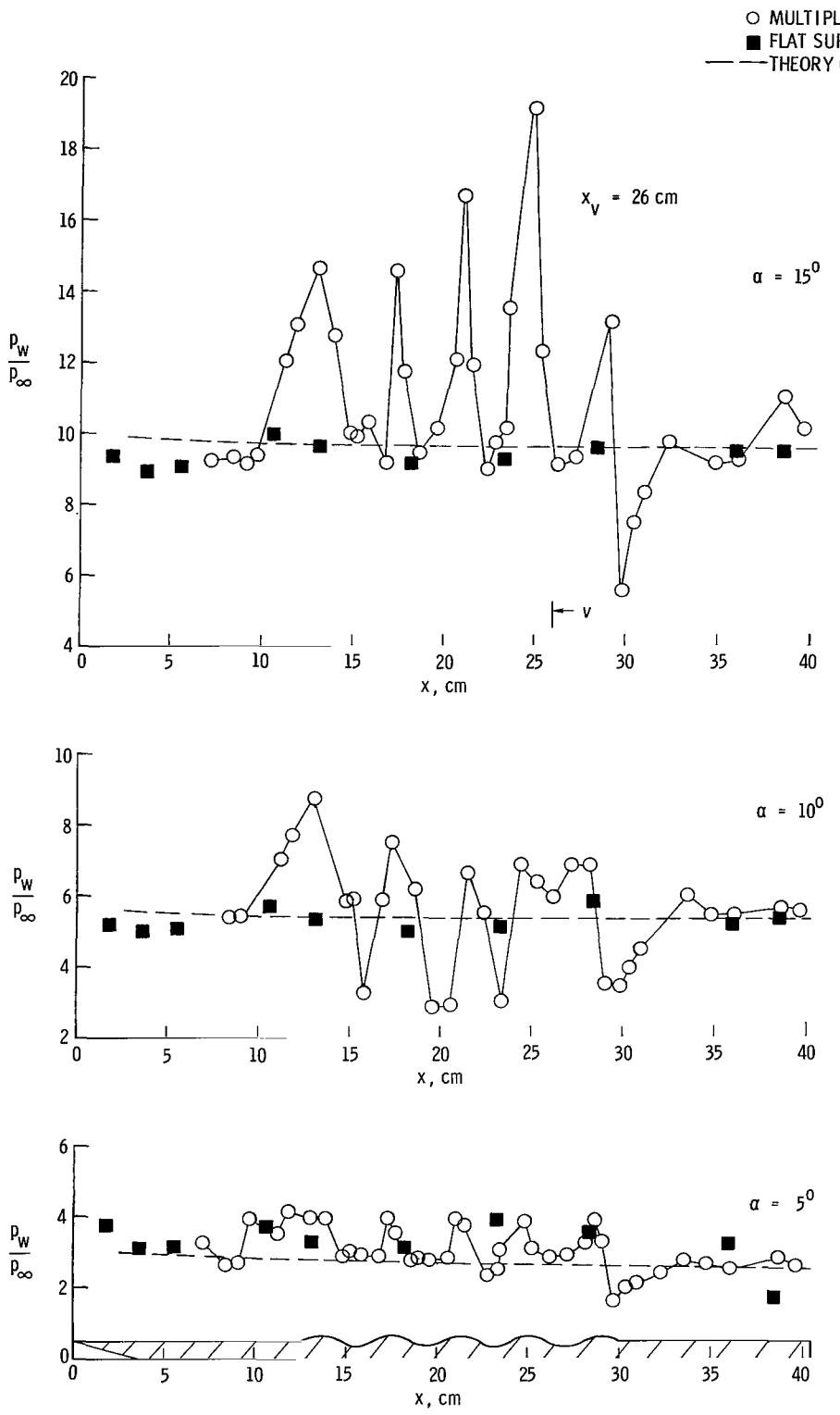

(a) $R_\infty = 0.032 \times 10^6$ per centimeter.

Figure 6.- Surface pressure distribution on sharp-leading-edge model. $M_\infty = 8.0$.

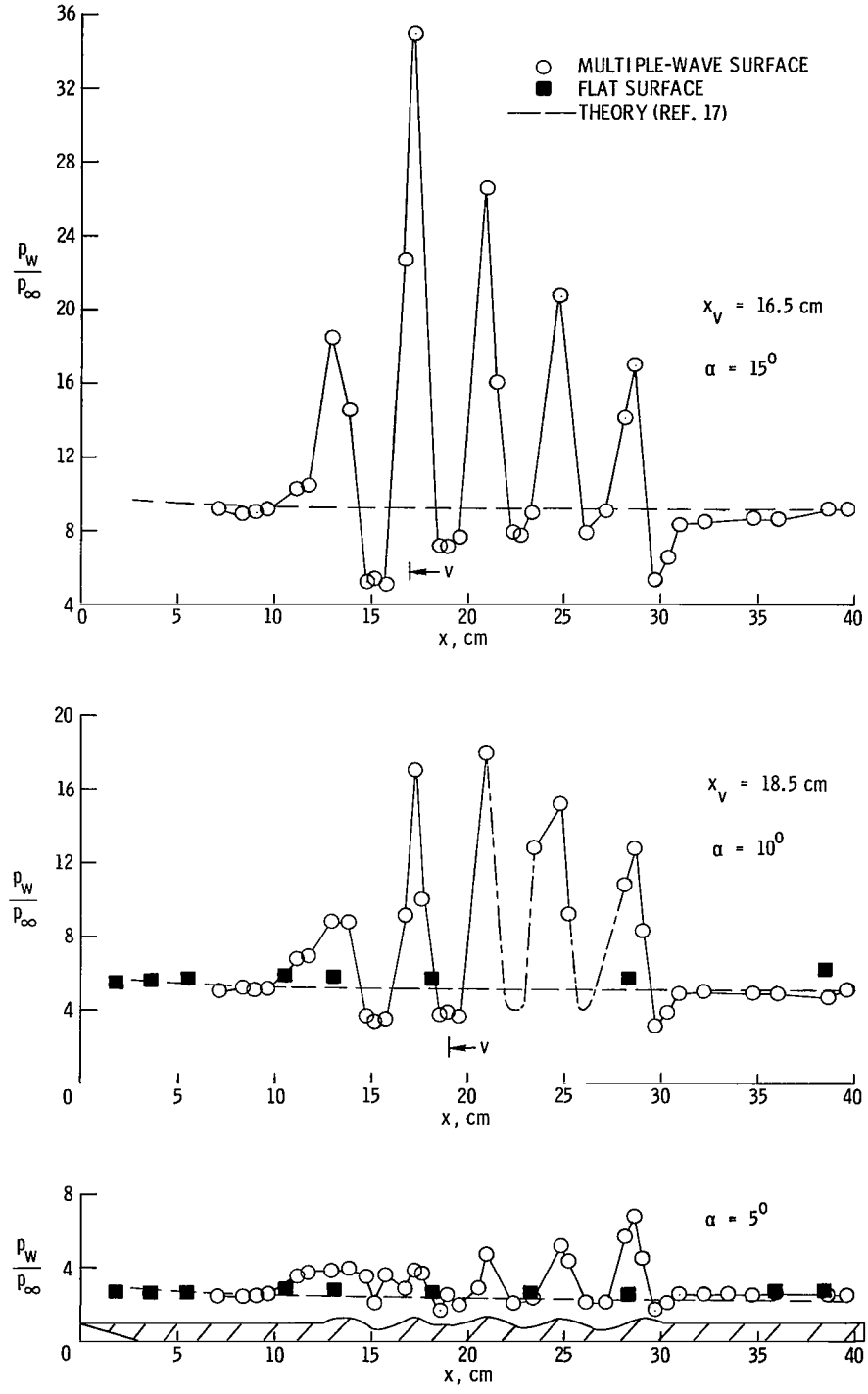

(b) $R_\infty = 0.13 \times 10^6$ per centimeter.

Figure 6.- Concluded.

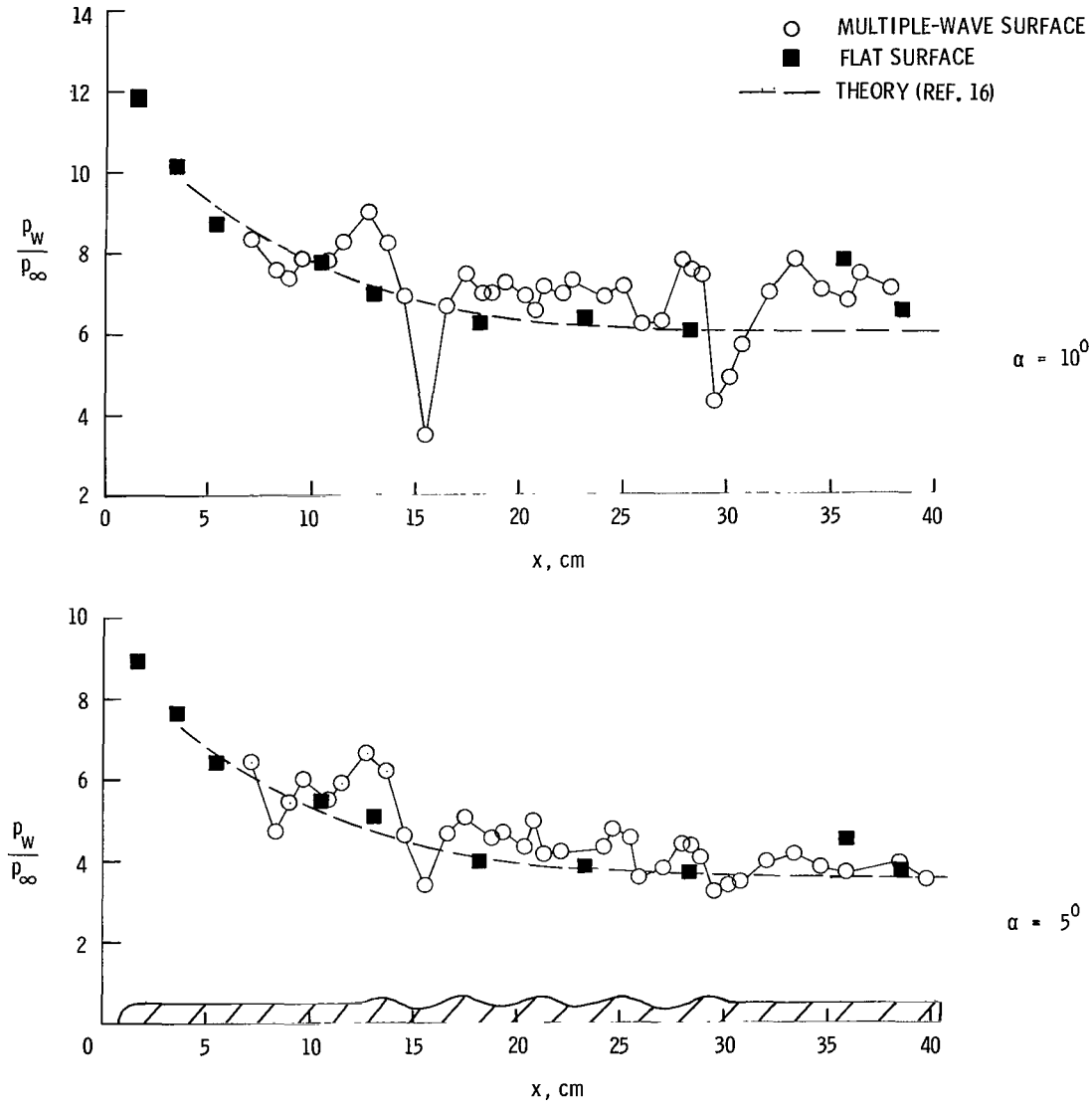

(a) $R_\infty = 0.032 \times 10^6$ per centimeter.

Figure 7.- Surface pressure distribution on blunt-leading-edge model. $M_\infty = 8.0$.

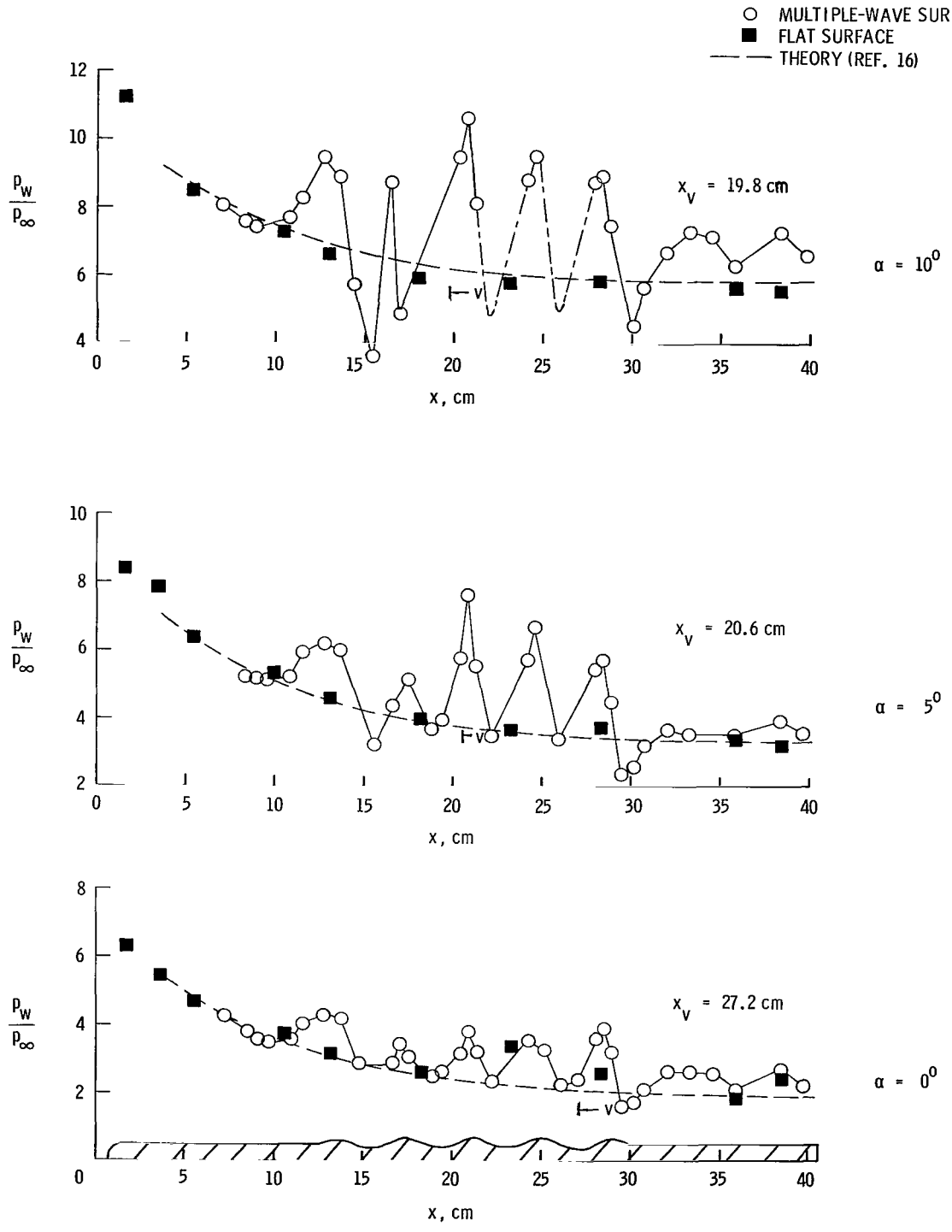

(b) $R_\infty = 0.13 \times 10^6$ per centimeter.

Figure 7.- Concluded.

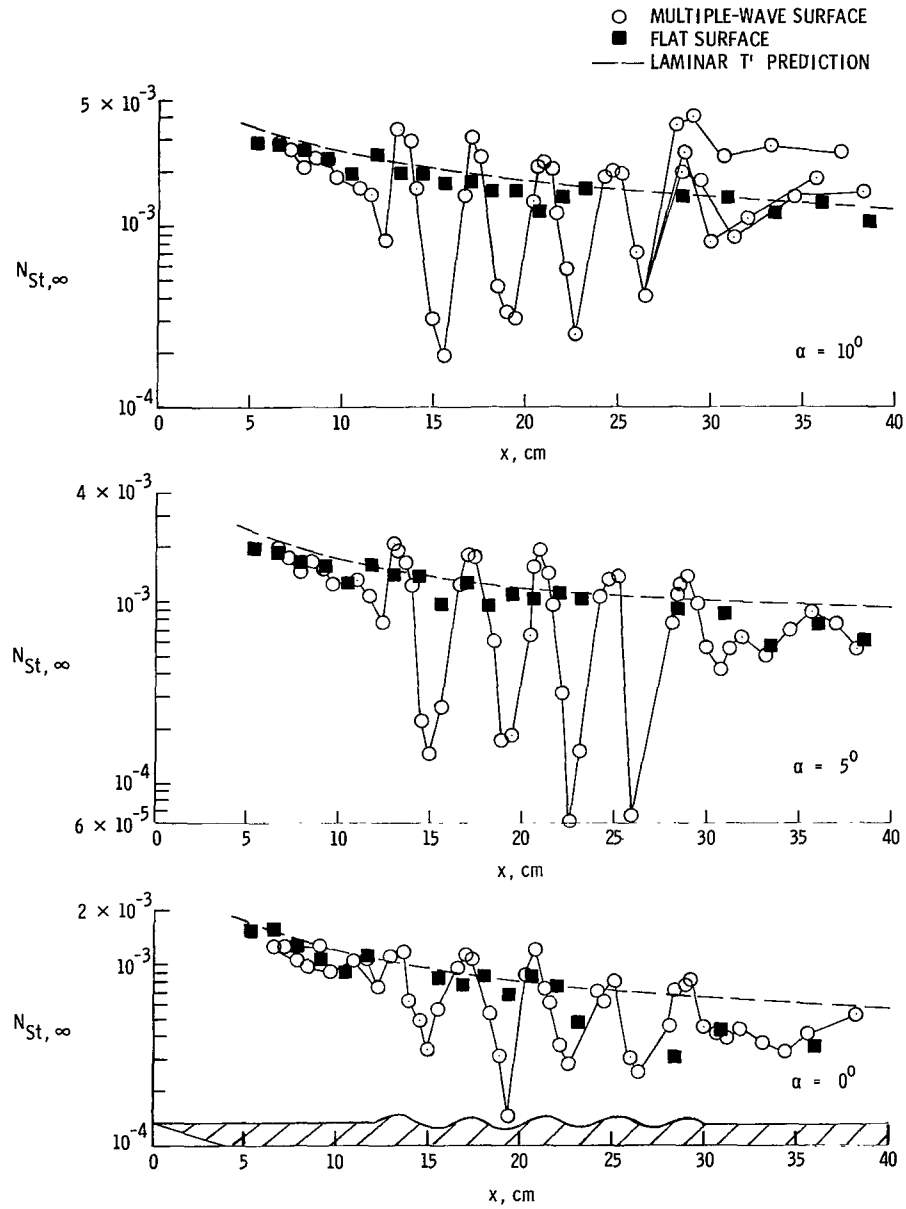

(a) $R_\infty = 0.0097 \times 10^6$ per centimeter.

Figure 8.- Surface heating distribution on sharp-leading-edge model. $M_\infty = 8.0$.

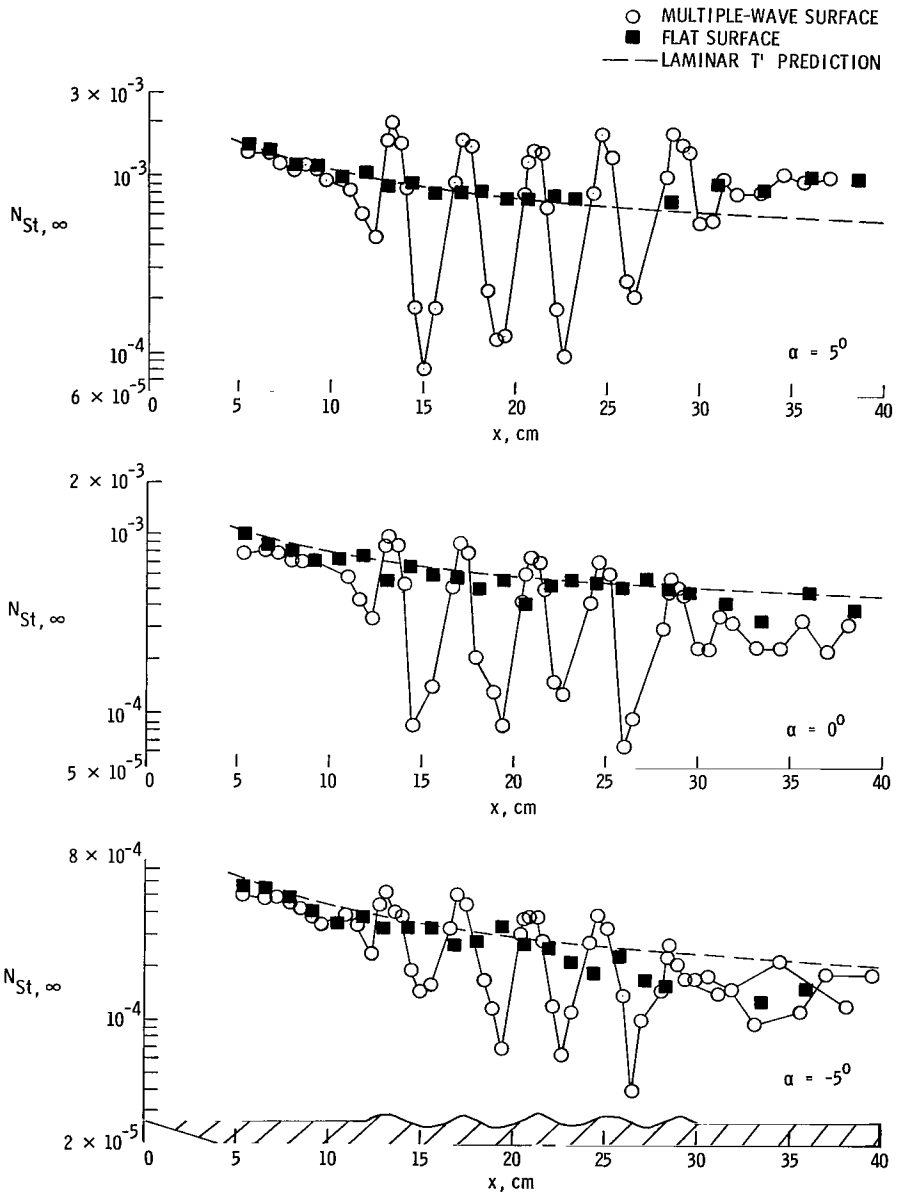

(b) $R_\infty = 0.032 \times 10^6$ per centimeter.

Figure 8.- Continued.

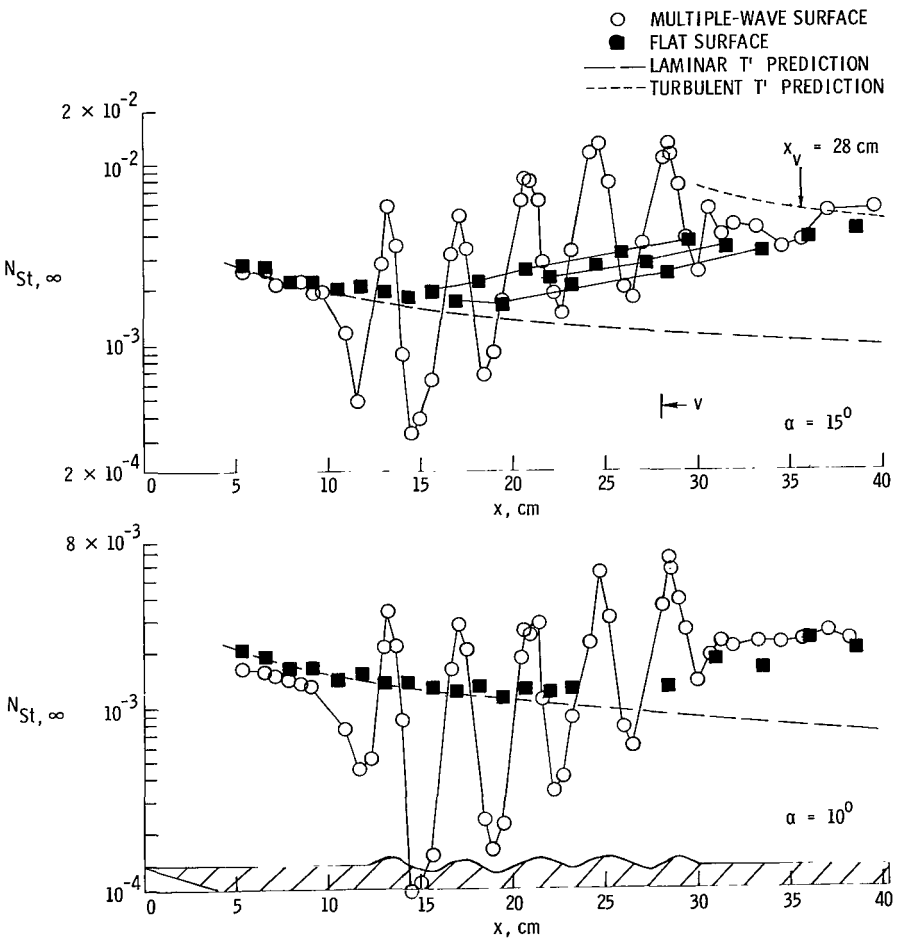

(b) Concluded.

Figure 8.- Continued.

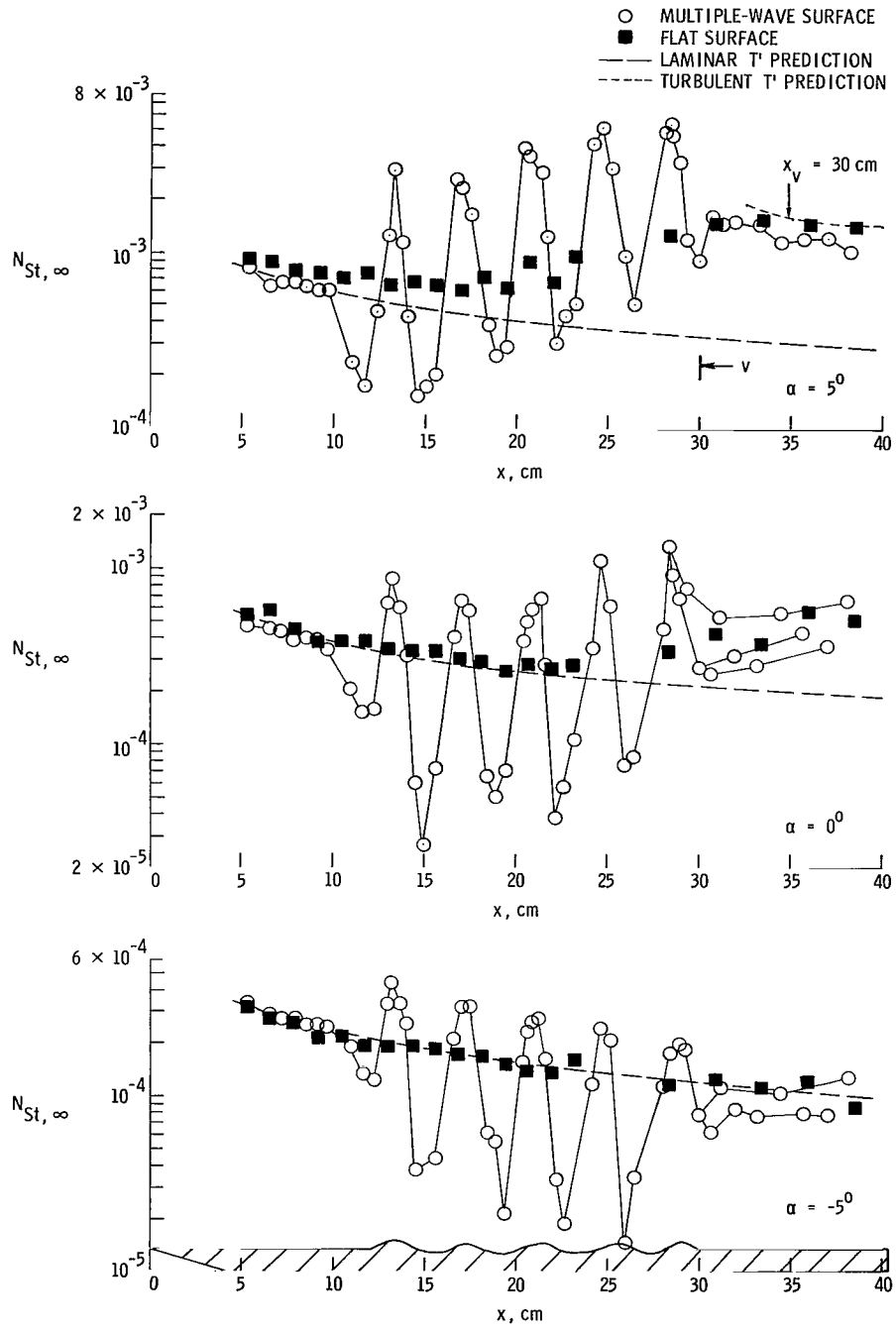

(c) $R_\infty = 0.11 \times 10^6$ per centimeter.

Figure 8.- Continued.

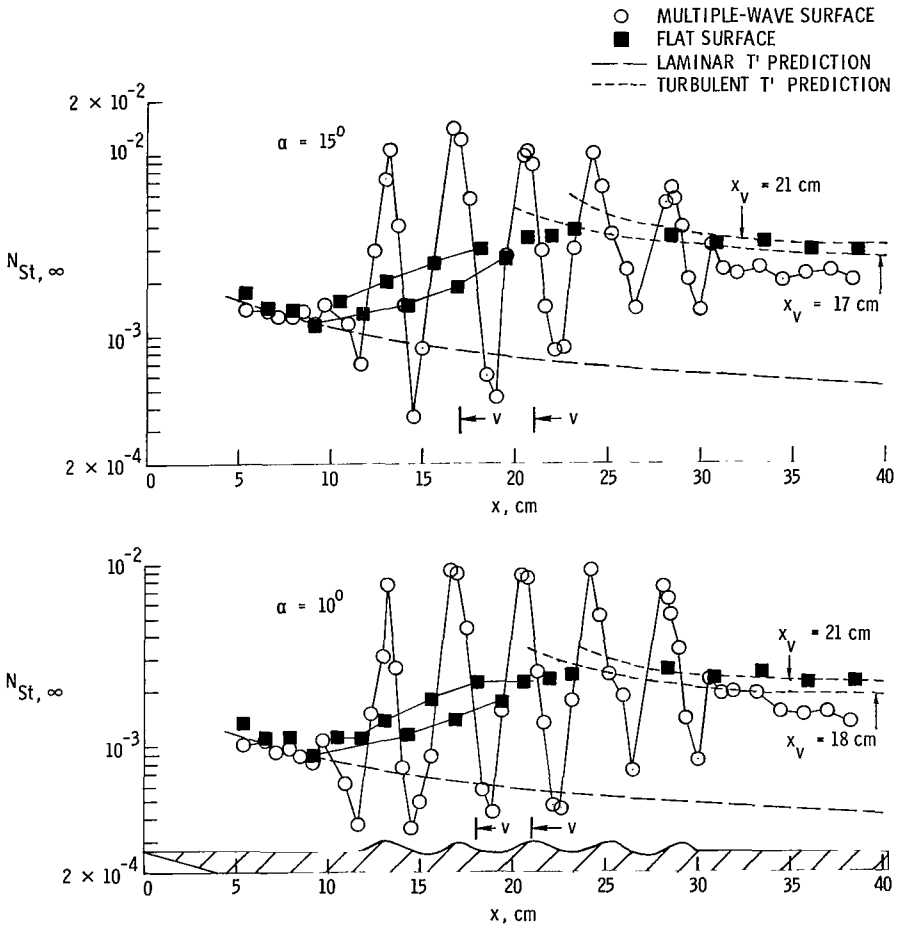

(c) Concluded.

Figure 8.- Continued.

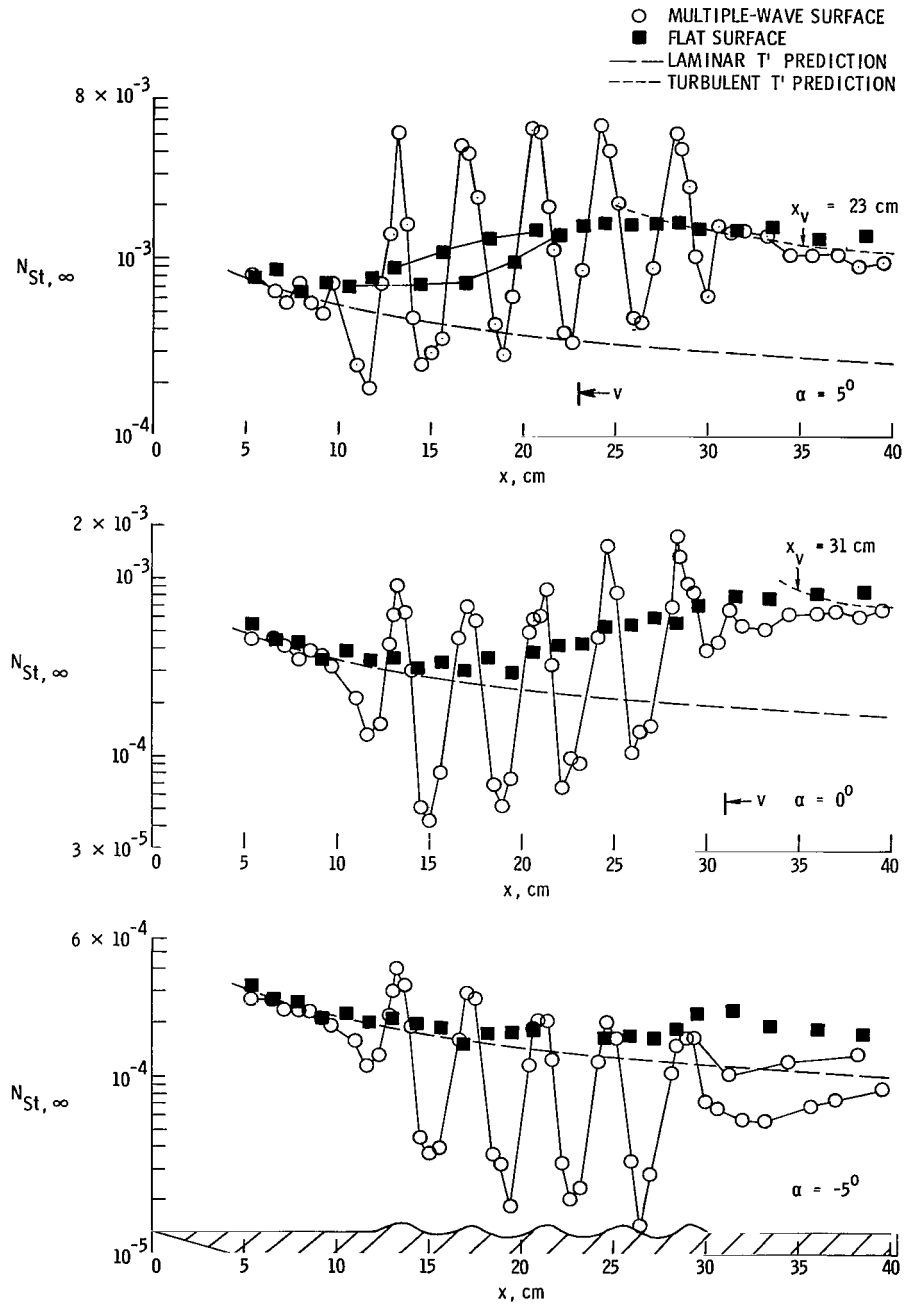

(d) $R_\infty = 0.13 \times 10^6$ per centimeter.

Figure 8.- Continued.

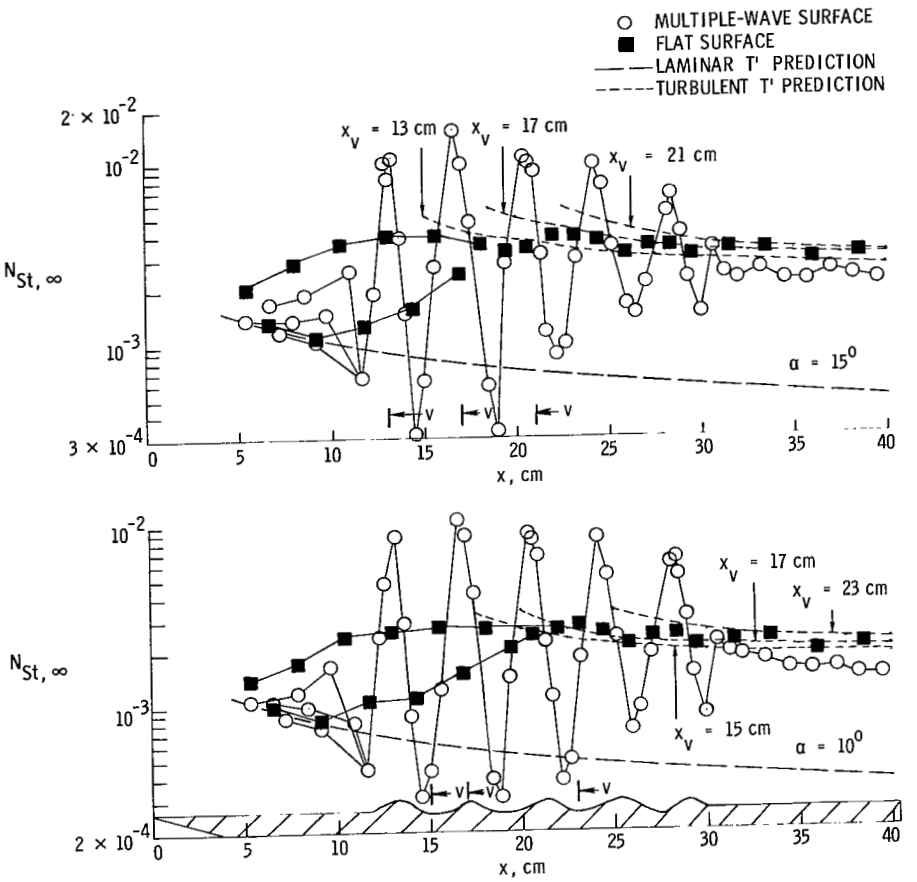

(d) Concluded.

Figure 8.- Continued.

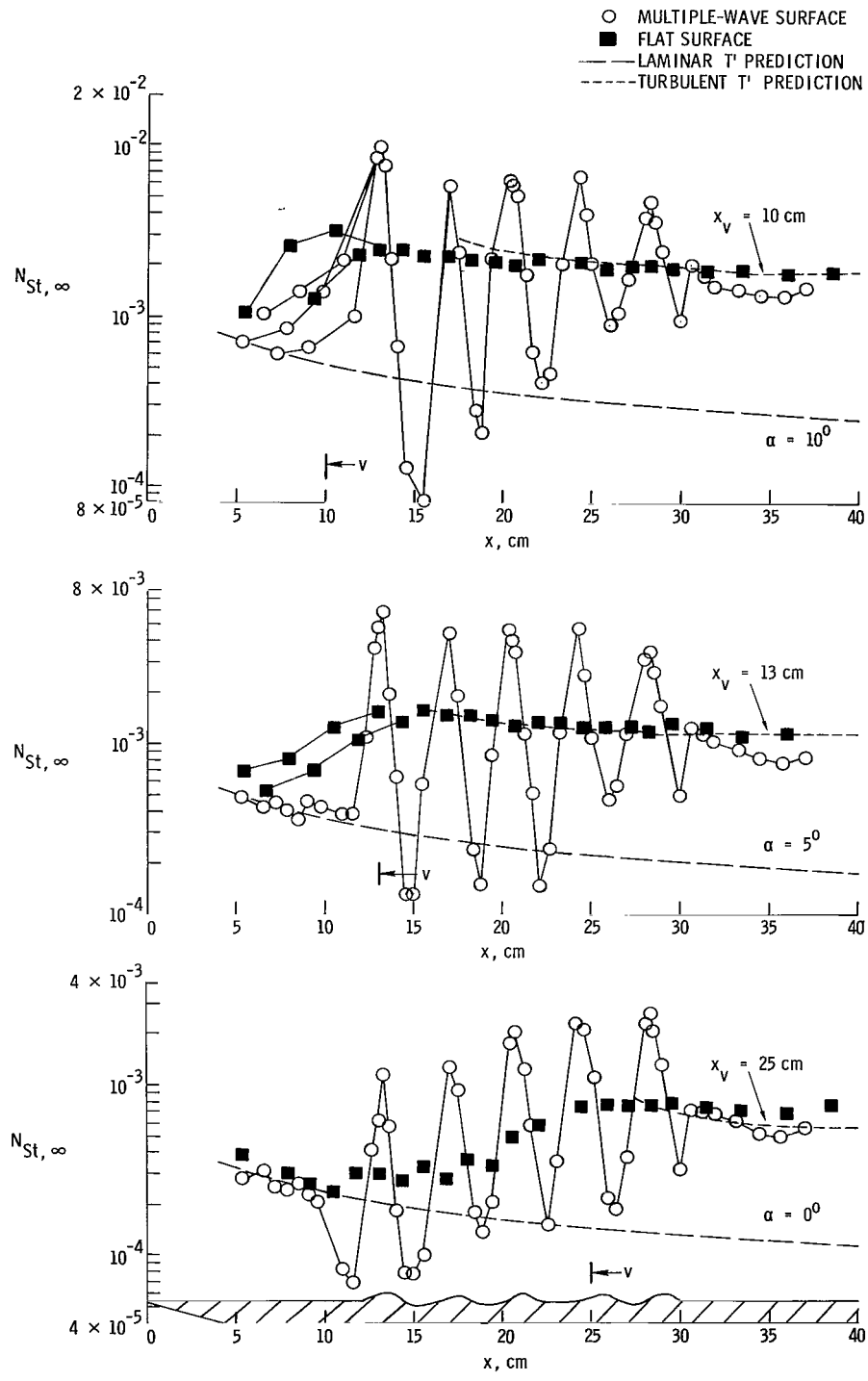

(e) $R_\infty = 0.29 \times 10^6$ per centimeter.

Figure 8.- Concluded.

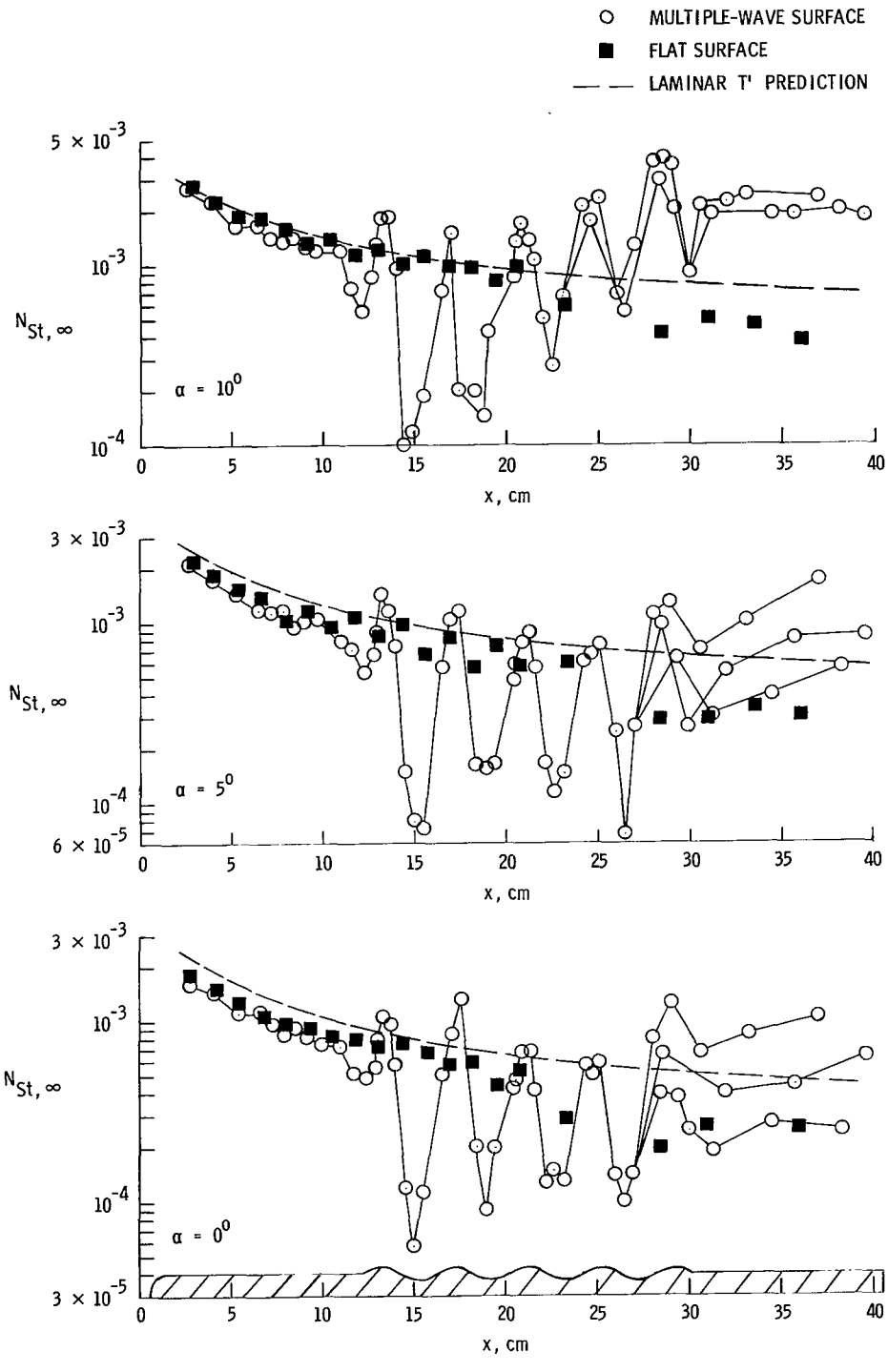

(a) $R_\infty = 0.032 \times 10^6$ per centimeter.

Figure 9.- Surface heating distribution on blunt-leading-edge model. $M_\infty = 8.0$.

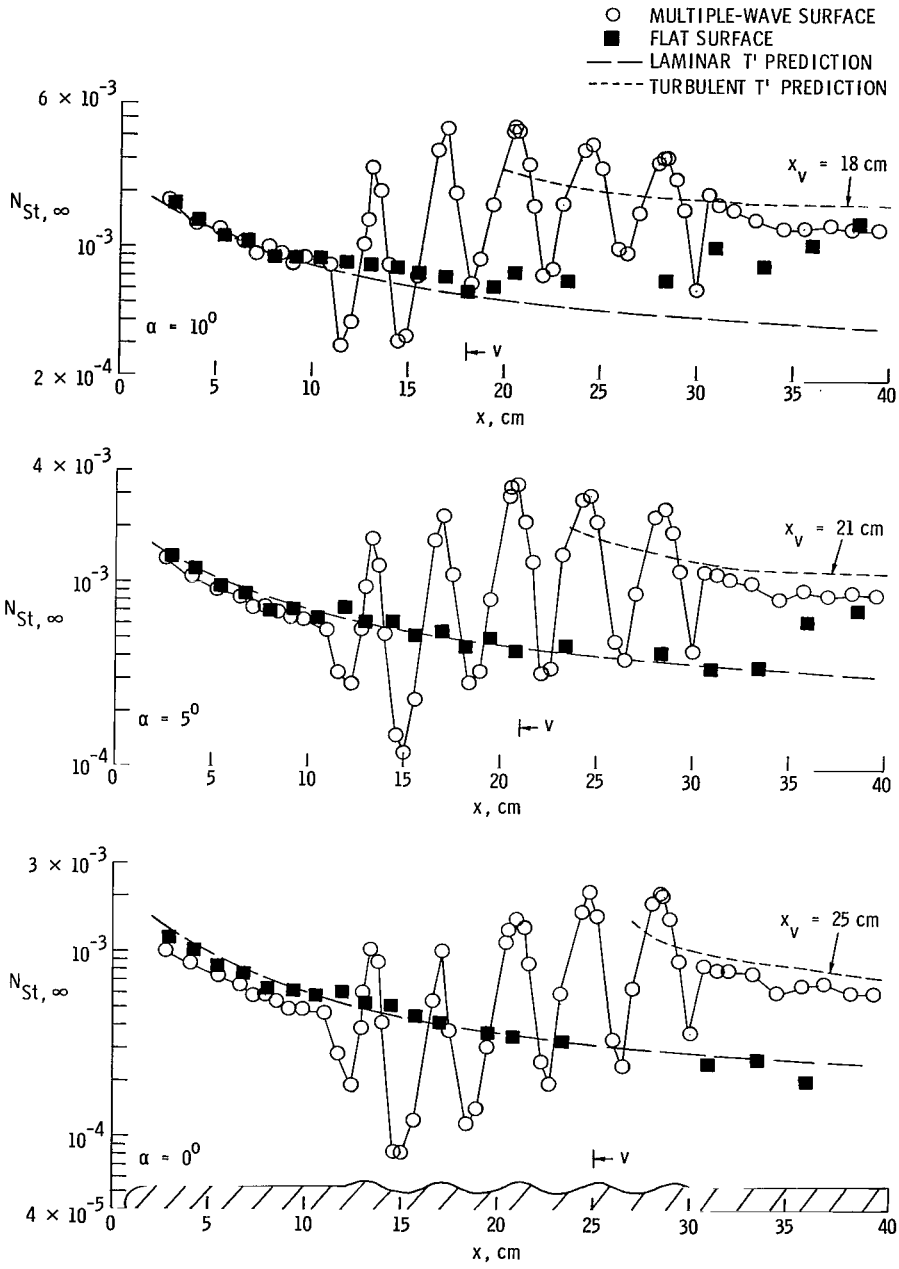

(b) $R_\infty = 0.11 \times 10^6$ per centimeter.

Figure 9.- Continued.

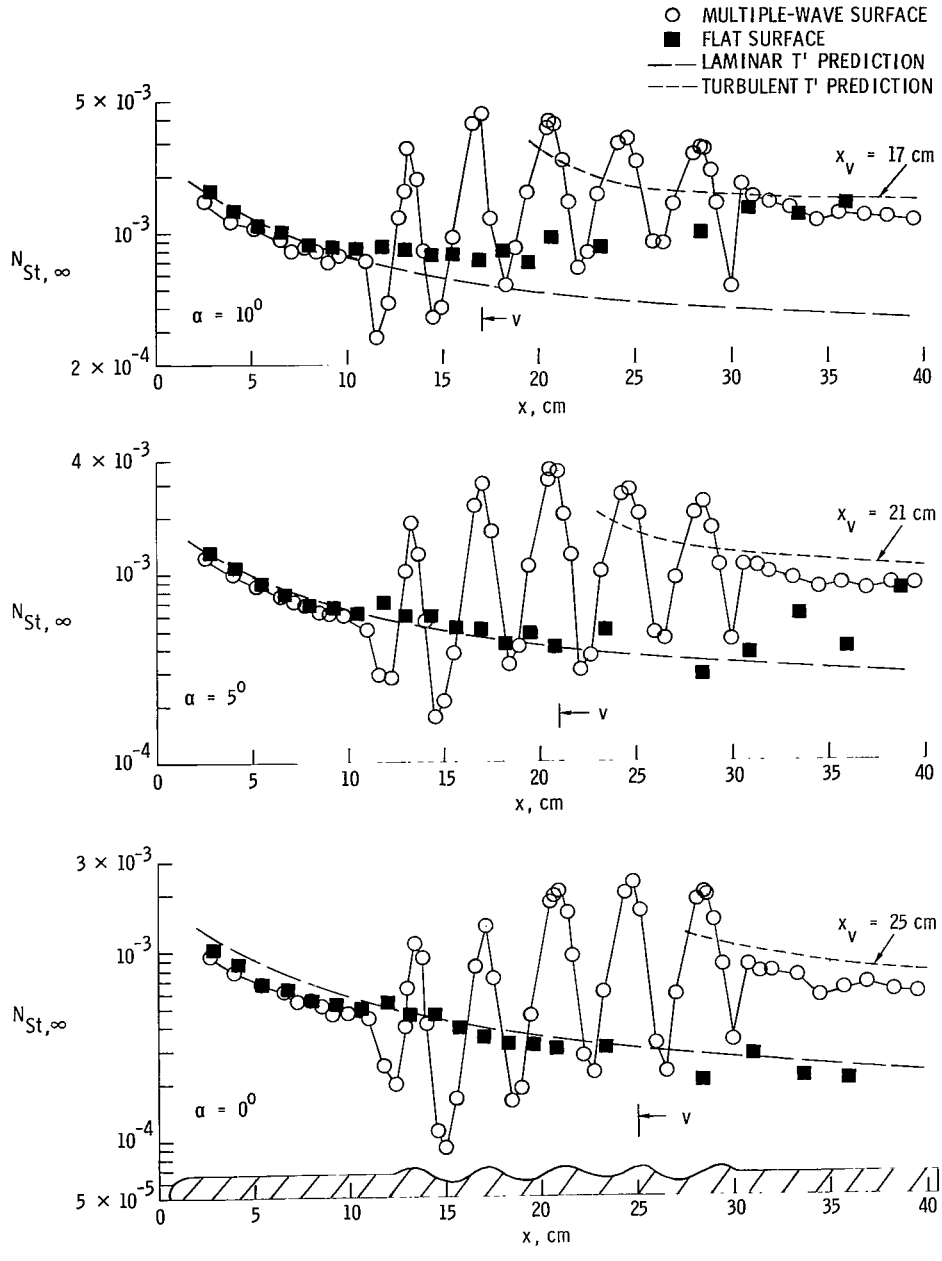

(c) $R_\infty = 0.13 \times 10^6$ per centimeter.

Figure 9.- Continued.

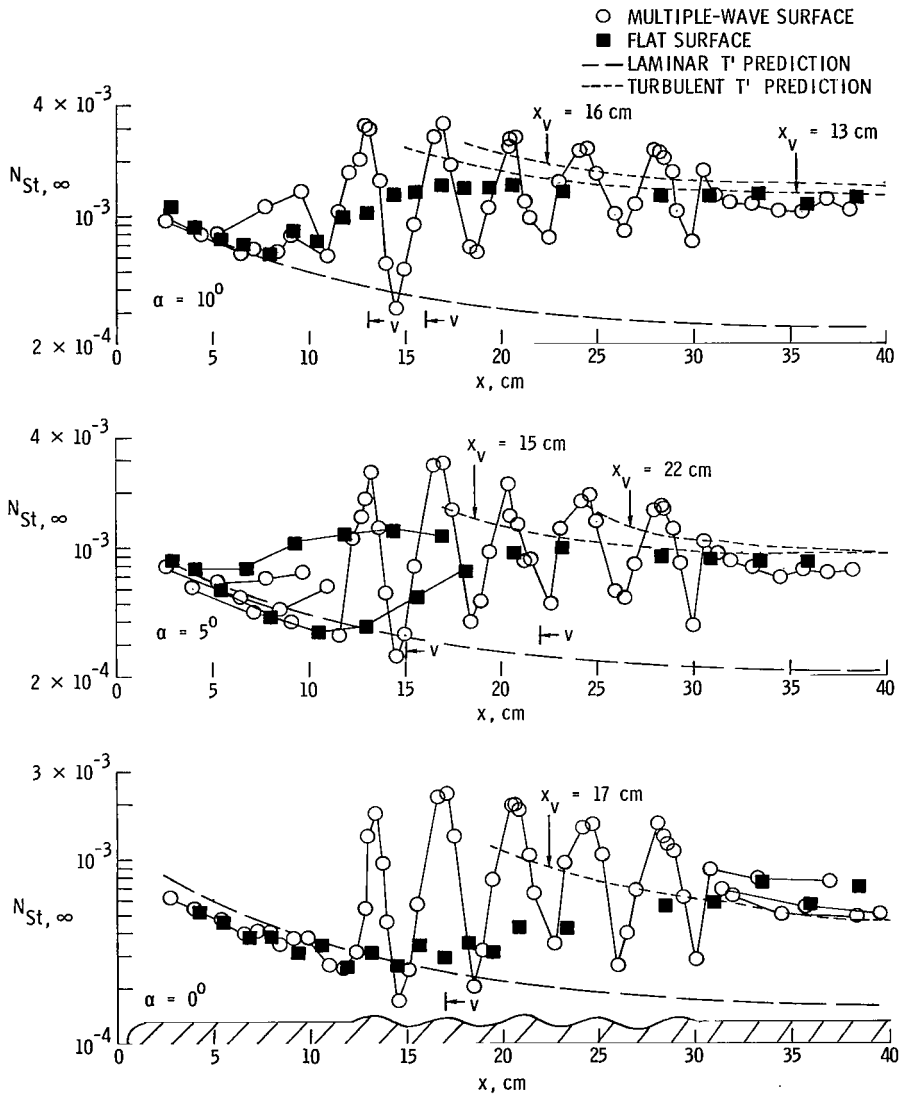

(d) $R_\infty = 0.29 \times 10^6$ per centimeter.

Figure 9.- Concluded.

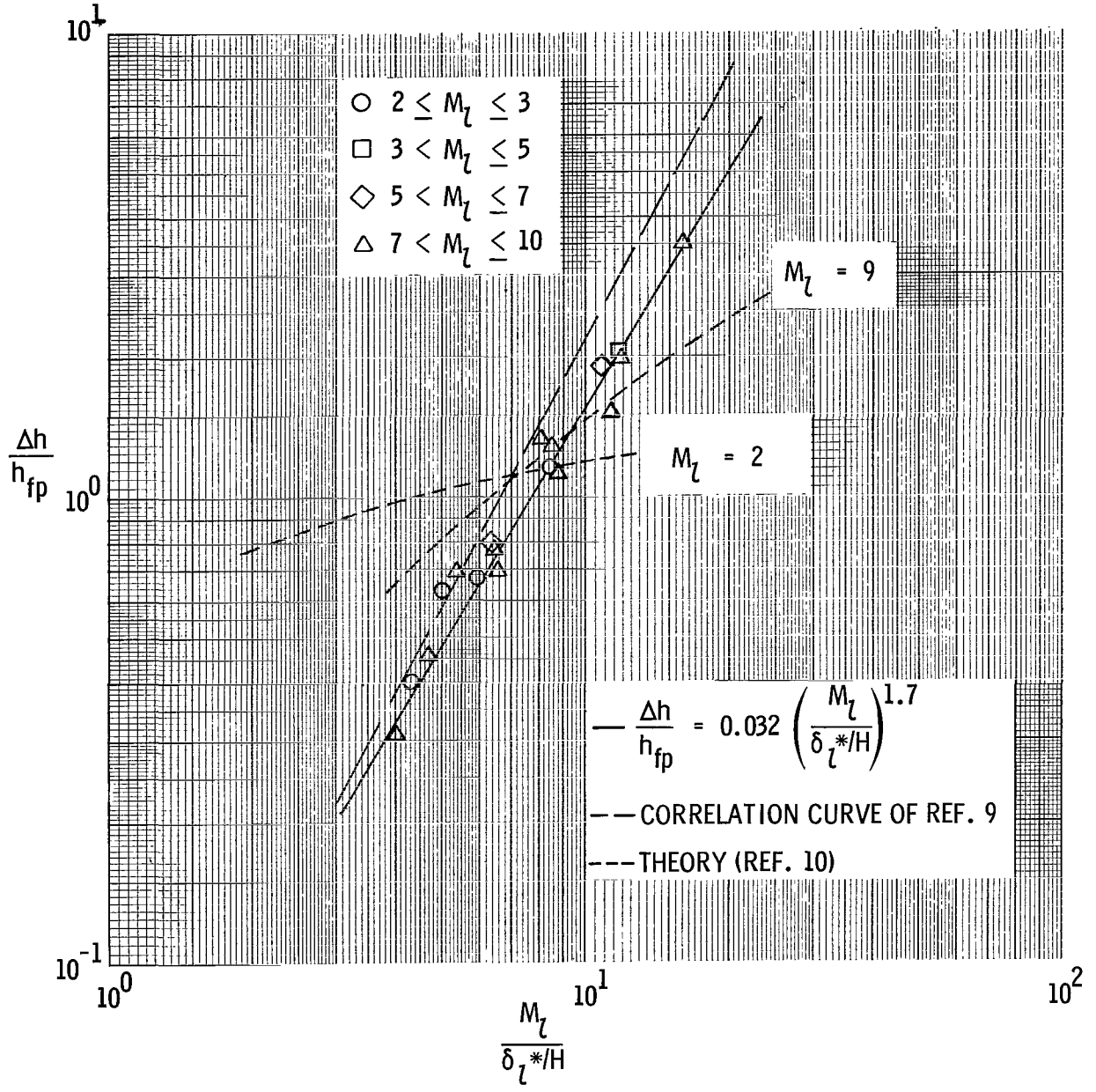

Figure 10.- Maximum heating on first wave peak in laminar flow. $M_\infty = 8.0$; $T_w/T_t = 0.4$; R_∞ varies from 0.0097×10^6 to 0.13×10^6 per centimeter.

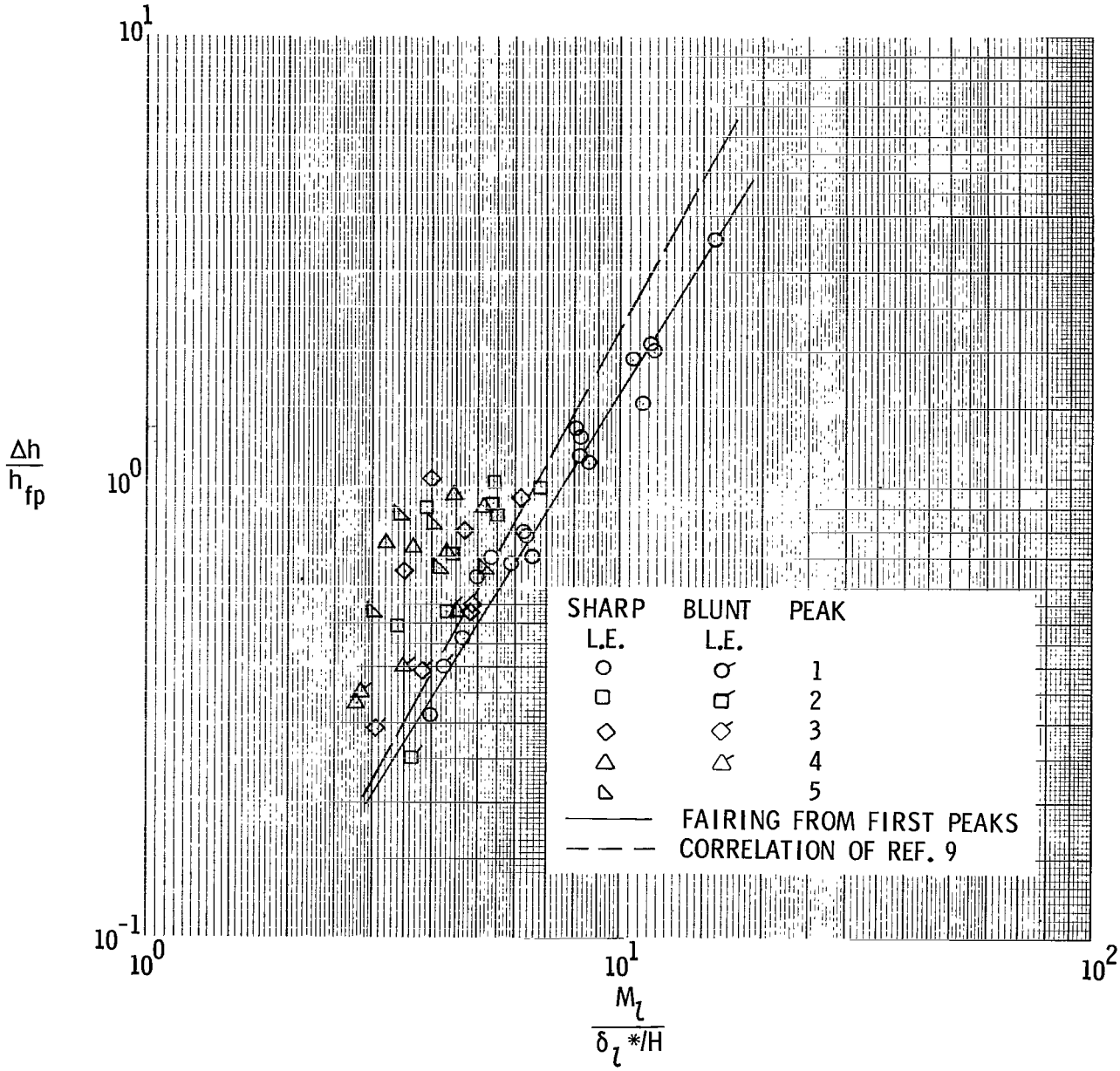

Figure 11.- Maximum heating over several wave peaks in laminar flow. $M_\infty = 8.0$; $T_w/T_t = 0.4$; R_∞ varies from 0.0097×10^6 to 0.13×10^6 per centimeter.

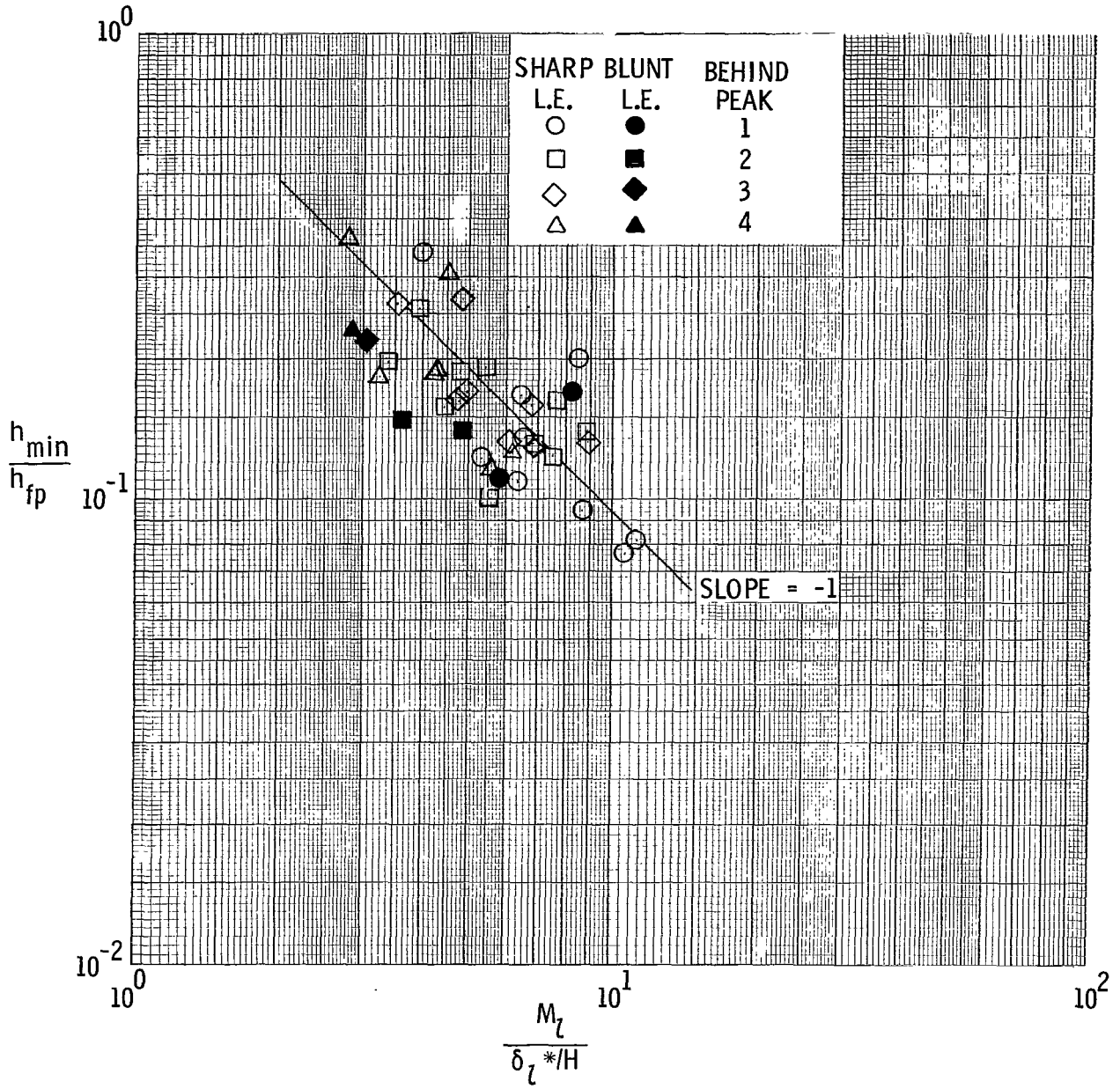

Figure 12.- Minimum heating behind wave peaks in laminar flow. $M_\infty = 8.0$. $T_w/T_t = 0.4$; R_∞ varies from 0.0097×10^6 to 0.13×10^6 per centimeter.

NASA-Langley, 1970 —— 12 L-5427

"The aeronautical and space activities of the United States shall be conducted so as to contribute . . . to the expansion of human knowledge of phenomena in the atmosphere and space. The Administration shall provide for the widest practicable and appropriate dissemination of information concerning its activities and the results thereof."

— NATIONAL AERONAUTICS AND SPACE ACT OF 1958

NASA SCIENTIFIC AND TECHNICAL PUBLICATIONS

TECHNICAL REPORTS: Scientific and technical information considered important, complete, and a lasting contribution to existing knowledge.

TECHNICAL NOTES: Information less broad in scope but nevertheless of importance as a contribution to existing knowledge.

TECHNICAL MEMORANDUMS: Information receiving limited distribution because of preliminary data, security classification, or other reasons.

CONTRACTOR REPORTS: Scientific and technical information generated under a NASA contract or grant and considered an important contribution to existing knowledge.

TECHNICAL TRANSLATIONS: Information published in a foreign language considered to merit NASA distribution in English.

SPECIAL PUBLICATIONS: Information derived from or of value to NASA activities. Publications include conference proceedings, monographs, data compilations, handbooks, sourcebooks, and special bibliographies.

TECHNOLOGY UTILIZATION PUBLICATIONS: Information on technology used by NASA that may be of particular interest in commercial and other non-aerospace applications. Publications include Tech Briefs, Technology Utilization Reports and Notes, and Technology Surveys.

Details on the availability of these publications may be obtained from:

SCIENTIFIC AND TECHNICAL INFORMATION DIVISION

NATIONAL AERONAUTICS AND SPACE ADMINISTRATION

Washington, D.C. 20546